CrossMark

REVIEW

Impinging of metallic nanoparticles along with the slip effects through a porous medium with MHD

Iqra shahzadi[1] · S. Nadeem[1]

Abstract The considered analysis comprises the effects of nanoparticles on the characteristics of the peristaltic flow through a homogeneous porous medium under the impact of magnetic field and slip effects by considering an appropriate mathematical model. Analysis is introduced by considering blood as the base fluid and metals such as copper and silver as the nanoparticles in the existence of the thermal and velocity slip effects. Lubrication approach is used to simplify the problem. Impact of related parameters on temperature, pressure rise, pressure gradient, velocity and streamlines are interpreted graphically. Comparison of the pure blood, silver blood and copper blood is presented and analyzed. It is also revealed that inclusion of nanoparticles scales down the velocity and temperature of fluid. Another valuable finding of the present investigation is that the silver nanoparticles enhance the pressure gradient when compared with the copper nanoparticles. Therefore, the current investigation is capable to achieve some essential and interesting characteristics in few biomedical applications.

Keywords Peristaltic flow · Copper and silver nanoparticles · Porous medium · Magnetic field · Slip effects

✉ Iqra shahzadi
  iqrashahzadiwah@gmail.com

1 Department of Mathematics, Quaid-i-Azam University, 45320, Islamabad 44000, Pakistan

1 Introduction

Flows in a tube or channel caused by sinusoidal waves generated along the channel walls are defined as peristaltic flows. It has abundant applications in physiology such as transport of bile, urine, chyme, food, male and female breeding cells through their specific tracks. Dialysis, heart–lung machines, roller, finger pumps and hose pumps are the engineering applications of peristalsis. Transit of sensitive and corrosive fluids is transported by means of peristalsis to prevent the direct influence towards the outer environment. Due to specific usefulness and immense continuation of peristaltic flows, various analyses are introduced to examine the peristalsis by considering distinct flow configurations [1–6]. Impact of external magnetic field is more useful, for instance, hyperthermia, reduction of bleeding during surgeries, drug carriers, advancement of magnetic devices utilizing magnetic particles and many others. Such biomedical applications motivate the researchers and, therefore, many theoretical investigations have been tackled to see the impact of magnetic field on peristaltic flows [7–10].

Beach sand, rye bread, human lung, wood and filter paper are the examples of naturally existing porous media. A superb biological illustration of a porous medium is the pharmaceutical position of gallstones when they decline into bile ducts and partially or completely close them. In recent years, many researchers have described the influence of porous medium on the flow by employing the Darcy's law [11–14]. Fluid bounded by vertical infinite plate and passing through the porous media has been investigated by Rapits et al. [15]. Varshney [16] has also considered the porous media with horizontal surface. Nonlinear peristaltic flow passing through porous inclined channel has been examined by Mekheimer [17]. Vasudev et al. [18] has

2 Springer

considered the vertical tube to discuss the impact of magnetic field and porous media.

Nanoparticle investigation is an area of impressive scientific interest in view of extensive range of promising utilization in biomedical, optical and electronic field. In the field of nanotechnology, a particle describes a small object which behaves like an individual in terms of its characteristic and transport. Nanotechnology introduced the creation and uses of different materials having the nanoscale levels of 1–100 nm to make products that exhibit peculiar properties. Implementation of nanotechnology in biomedical applications giving exclusive physical and chemical property has the capability to give strongly improved distinguishing methods and efficient mechanism for molecular liability [19–23]. This new kind of nanotechnology was first introduced by Choi and Eastman [24]. Buongiorno [25] showed that Brownian motion and thermophoresis effects are significant in the dynamics of nanofluids. Later on, Akbar [26] investigated the impact of nanoparticles on incompressible viscous fluid by considering asymmetric channel. Nadeem and Shahzadi [27] analyzed the two-phase nanofluid in a curved channel. Nanoparticles with exclusive properties has earned much consideration from researchers and extensive studies investigate the influence of nanotechnology in various applications available in the literature such as [28–32].

The mechanics of peristaltic flow through different configuration with no slip condition have been elaborated by various researchers in which they stimulate that the fluid film moves with closest to the boundary surface [33, 34]. It is now acceptable fact that the fluid flow through all tubular organs in human body are inwardly laminated with secretion layers and mucus. These layers consecutively avoid the fluid from sticking to the tube walls. In this aspect no slip condition is valid between the solid boundary and fluid. The important applications of boundary slip conditions are in polishing valves of fabricated hearts and internal cavities. With such motivation, some researchers investigated the slip effects on the peristaltic flow of commonly used fluids [35, 36]. Yıldırım and Sezer [37] examined the influence of partial slip condition on MHD viscous fluid by assuming asymmetric channel.

The aspiration of present analysis is to investigate the impinging of metallic nanoparticles on magneto hydrodynamic flow through a uniform porous medium with slip effects. Indeed, the magnetic nanofluid has both the prospects of liquid and magnetic field. Such fluids have beneficial applications related to modulators, adjustable optical fiber filters, optical gratings and switches. Magnetic nanoparticles have significant importance in cancer therapy, medicine and to instruct the particles to move along the blood stream towards the tumor with magnets. In hyperthermia, contrast improvement in magnetic

resonance and drug delivery, the magneto nanofluids have significant importance. The influence of magnetic nanoparticles on the tumor cells has been found in more adhesive than invigorating cells. Here, for the present analysis we have used copper (Cu) and silver (Ag) nanoparticles. Magnetic properties of nanoparticles add a new extent where they can enhance the application of an external magnetic field. Thermophysical properties of the nanofluids such as effective viscosity, density, electric conductivity and thermal conductivity are taken into account. By employing the approximation of long wavelength and low Reynolds number, the mathematical model is presented. Resulting equations are solved exactly. Physical clarification of results is interpreted by means of graphs and tables.

2 Formulation of the problem

We have considered the vertical tube of width $2a$ for peristaltic flow of nanofluid through a homogenous porous medium under velocity and thermal slip effects. A nanofluid flow phenomenon is consisting of blood with copper/silver as the nanoparticles. An external magnetic field of strength B_0 is applied and effects of induced magnetic field are neglected for low magnetic Reynolds number condition. It is supposed that the thermal equilibrium is maintained between the base fluid and the nanoparticles. The coordinates (R, Z) are elected in such a way that R-axis is along the radial direction and Z-axis lies along the length of the tube. Furthermore, walls of tube are preserved at a constant temperature of T_0. A sinusoidal wave of small amplitude b and wavelength moves down the walls with constant speed c. Flow in the tube is generated
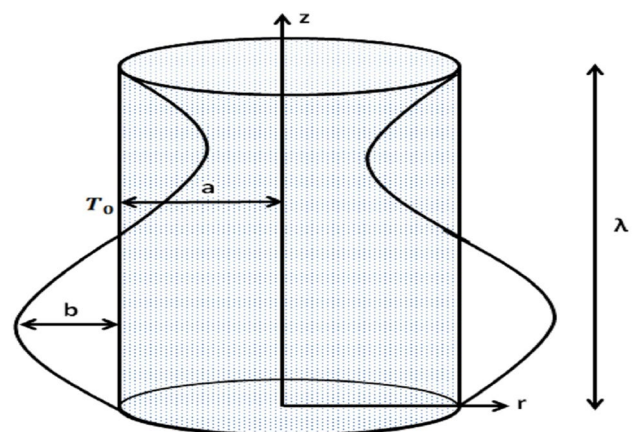

Fig. 1 Geometrical sketch

by these waves. Schematic geometrical sketch is represented in Fig. 1.

The shape of traveling waves is represented as:

$$\bar{H}(\bar{t}, \bar{Z}) = b \sin\left[(\bar{Z} - c\bar{t}) \frac{2\pi}{\lambda} \right] + a, \tag{1}$$

In Eq. (1), amplitude of the wave is expressed by b, width of the tube is expressed by a, wave speed is expressed by c and wavelength is expressed by λ.

The two-dimensional continuity equation for incompressible fluid is defined below

$$\frac{\bar{U}}{\bar{R}} + \frac{\partial \bar{U}}{\partial \bar{R}} + \frac{\partial \bar{W}}{\partial \bar{Z}} = 0, \tag{2}$$

in which $\bar{W}$ and $\bar{U}$ represent the transverse and longitudinal components of velocity in the laboratory frame. The $\bar{R}$ and $\bar{Z}$ components of momentum equation in the presence of mixed convection are [5–11]

$$
\rho_{\text{nf}} \left(\frac{\partial \bar{U}}{\partial \bar{R}} \bar{U} + \frac{\partial \bar{U}}{\partial \bar{Z}} \bar{W} + \frac{\partial \bar{U}}{\partial \bar{t}} \right)
$$
$$
= \mu_{\text{nf}} \left(\frac{\partial^2 \bar{U}}{\partial \bar{Z}^2} + \frac{1}{\bar{R}} \frac{\partial \bar{U}}{\partial \bar{R}} + \frac{\partial^2 \bar{U}}{\partial \bar{R}^2} - \frac{\bar{U}}{\bar{R}^2} \right) \tag{3}
$$
$$
- \frac{\mu_{\text{nf}}}{K_1} \bar{U} + (\rho\alpha)_{\text{nf}} g(\bar{T} - T_0) - \frac{\partial \bar{P}}{\partial \bar{R}},
$$

$$
\rho_{\text{nf}} \left(\frac{\partial \bar{W}}{\partial \bar{R}} \bar{U} + \frac{\partial \bar{W}}{\partial \bar{t}} + \frac{\partial \bar{W}}{\partial \bar{Z}} \bar{W} \right)
$$
$$
= \mu_{\text{nf}} \left(\frac{\partial^2 \bar{W}}{\partial \bar{Z}^2} + \frac{1}{\bar{R}} \frac{\partial \bar{W}}{\partial \bar{R}} + \frac{\partial^2 \bar{W}}{\partial \bar{R}^2} \right) - \sigma_{\text{nf}} B_0^2 \bar{W} \tag{4}
$$
$$
- \frac{\mu_{\text{nf}}}{K_1} \bar{W} + (\rho\alpha)_{\text{nf}} g(\bar{T} - T_0) - \frac{\partial \bar{P}}{\partial \bar{Z}}.
$$

Energy equation in the presence of heat generation is defined by

$$
(\rho C_p)_{\text{nf}} \left(\frac{\partial \bar{T}}{\partial \bar{R}} \bar{U} + \frac{\partial \bar{T}}{\partial \bar{Z}} \bar{W} + \frac{\partial \bar{T}}{\partial \bar{t}} \right)
$$
$$
= K_{\text{nf}} \left(\frac{\partial^2 \bar{T}}{\partial \bar{Z}^2} + \frac{\partial^2 \bar{T}}{\partial \bar{R}^2} + \frac{1}{\bar{R}} \frac{\partial \bar{T}}{\partial \bar{R}} \right) + Q_0. \tag{5}
$$

In the above equations, $\bar{T}$ is the temperature of the fluid, K_1 is the permeability of the porous medium, $\bar{P}$ is the pressure, B_0 is the magnetic field strength, Q_0 is the constant heat absorption and generation. For the proposed nanofluid model, ρ_{nf} is the density of the nanofluid, μ_{nf} is the variable nanofuid viscosity, α_{nf} is the thermal expansion coefficient, σ_{nf} is the electrical conductivity of the nanofluid, K_{nf} is the thermal conductivity of the nanofluid and $(\rho C_p)_{\text{nf}}$ is the nanofluid heat capacitance.

In this investigation, we have utilized the relation given by Brinkman [22] as,

Table 1 Thermophysical parameters of blood, silver and copper [31]

Physical properties	Blood	Silver	Copper
c_p (J/kg K)	3594	235	385
K (W/m K)	0.492	385	400
ρ (kg/m³)	1063	10,500	8933
$\alpha \times 10^{-5}$ (1/K)	0.18	1.87	1.67
σ (S/m)	6.67×10^{-1}	6.3×10^7	5.96×10^7

$$\mu_{\text{nf}} = \frac{\mu_{\text{f}}}{(1 - \varphi)^{2.5}}. \tag{6}$$

The effective density, electrical conductivity, thermal conductivity and specific heat of nanofluid are defined as [23],

$$(\rho c_p)_{\text{nf}} = \phi(\rho c_p)_{\text{s}} + (1 - \phi)(\rho c_p)_{\text{f}}, \alpha_{\text{nf}} = \frac{K_{\text{nf}}}{(\rho C_p)_{\text{nf}}}, \tag{7}$$

$$(\rho\alpha)_{\text{nf}} = \phi(\rho\alpha)_{\text{s}} + (1 - \phi)(\rho\alpha)_{\text{f}},$$
$$\frac{\sigma_{\text{nf}}}{\sigma_{\text{f}}} = 1 + \frac{3\left(\frac{\sigma_{\text{s}}}{\sigma_{\text{f}}} - 1\right)\phi}{\left(\frac{\sigma_{\text{s}}}{\sigma_{\text{f}}} + 2\right) - \left(\frac{\sigma_{\text{s}}}{\sigma_{\text{f}}} - 1\right)\phi},$$
$$\frac{K_{\text{nf}}}{K_{\text{f}}} = \frac{2k_{\text{f}} + k_{\text{s}} + 2\phi(k_{\text{s}} - k_{\text{f}})}{2k_{\text{f}} + k_{\text{s}} + \phi(k_{\text{f}} - k_{\text{s}})},$$
$$\rho_{\text{nf}} = \phi\rho_{\text{s}} + (1 - \phi)\rho_{\text{f}}, \tag{8}$$

Here effective thermal conductivity of the nanofluid is given by Maxwell–Gamett's (MG-model). For the base fluid ρ_{f} is the density, α_{f} is thermal expansion coefficient, μ_{f} is the viscosity, K_{f} is the thermal conductivity and $(\rho c_p)_{\text{f}}$ is heat capacitance for the base fluid while ρ_{s} is the density, $(\rho c_p)_{\text{s}}$ is heat capacitance, k_{s} is thermal conductivity, α_{s} is thermal expansion coefficient and ϕ is the volume fraction of nanoparticles. The experimental values of these physical parameters are presented in Table 1.

In the fixed frame the velocity and the thermal slip conditions are defined as [35–37]

$$\frac{\partial \bar{W}}{\partial \bar{R}} = 0, \quad \bar{T} = \bar{T}_0, \quad \text{at } \bar{R} = 0, \tag{9}$$

$$\bar{W} - \bar{W}_w = -\delta_1 \tau_{\bar{R}\bar{Z}}, \quad \bar{T} - \bar{T}_w = -\beta_1 \frac{\partial \bar{T}}{\partial \bar{R}}, \quad \text{at } \bar{R} = \bar{H}(\bar{Z}, t), \tag{10}$$

where $\tau_{\bar{R}\bar{Z}}$ is the extra stress tensor, $\bar{T}_w$ is the temperature which is equal to $\bar{T}_0$, α_1 is the velocity slip and β_1 is the thermal slip parameter.

The following transformation is used to swap from fixed frame $(\bar{R}, \bar{Z}, \bar{t})$ to wave frame $(\bar{r}, \bar{z})$,

$$\bar{Z} = \bar{z} + c\bar{t}, \quad \bar{p}(\bar{z}, \bar{r}) = \bar{P}(\bar{Z}, \bar{R}, \bar{t}),$$
$$\bar{w} = \bar{W} - c, \quad \bar{R} = \bar{r}, \quad \bar{u} = \bar{U}, \tag{11}$$

2538

J Braz. Soc. Mech. Sci. Eng. (2017) 39:2535–2560

in which $\bar{p}$ is the pressure and $\bar{u}$ and $\bar{w}$ are the velocity components. Equations (2)–(5) through Eqs. (6)–(11) give,

$$\frac{\partial \bar{w}}{\partial \bar{z}} + \frac{\partial \bar{u}}{\partial \bar{r}} + \frac{\bar{u}}{\bar{r}} = 0, \tag{12}$$

$$\begin{aligned}
&((1-\phi)\rho_f + \varphi\rho_s)\left(\frac{\partial \bar{u}}{\partial \bar{r}}\bar{u} - \frac{\partial \bar{u}}{\partial \bar{z}}c + \frac{\partial \bar{u}}{\partial \bar{z}}(\bar{w}+c)\right) \\
&= \frac{\mu_f}{(1-\phi)^{2.5}}\left(\frac{1}{\bar{r}}\frac{\partial \bar{u}}{\partial \bar{r}} + \frac{\partial^2 \bar{u}}{\partial \bar{r}^2} - \frac{\bar{u}}{\bar{r}^2} + \frac{\partial^2 \bar{u}}{\partial \bar{z}^2}\right) \\
&\quad + (1-\phi)(\rho\alpha)_f + \phi(\rho\alpha)_s g(T-T_0) \\
&\quad - \frac{\mu_{nf}}{K_1}(\bar{u}+c) - \frac{\partial \bar{p}}{\partial \bar{r}},
\end{aligned} \tag{13}$$

$$\begin{aligned}
&((1-\phi)\rho_f + \phi\rho_s)\left(\frac{\partial \bar{w}}{\partial \bar{r}}\bar{u} - \frac{\partial \bar{w}}{\partial \bar{z}}c + \frac{\partial \bar{w}}{\partial \bar{z}}(\bar{w}+c)\right) \\
&= \frac{\mu_f}{(1-\phi)^{2.5}}\left(\frac{1}{\bar{r}}\frac{\partial \bar{w}}{\partial \bar{r}} + \frac{\partial^2 \bar{w}}{\partial \bar{r}^2} + \frac{\partial^2 \bar{w}}{\partial \bar{z}^2}\right) \\
&\quad + (1-\phi)(\rho\alpha)_f + \phi(\rho\alpha)_s g(T-T_0) \\
&\quad - \sigma_{nf}B_0^2(\bar{w}+c) - \frac{\mu_{nf}}{K_1}(\bar{w}+c) \\
&\quad - \frac{\partial \bar{p}}{\partial \bar{z}},
\end{aligned} \tag{14}$$

$$\begin{aligned}
&\left(\frac{\partial \bar{T}}{\partial \bar{r}}\bar{u} - \frac{\partial \bar{T}}{\partial \bar{z}}c + \frac{\partial \bar{T}}{\partial \bar{z}}(\bar{w}+c)\right) \\
&= \frac{Q_0}{(1-\phi)(\rho c_p)_f + \phi(\rho c_p)_s} \\
&\quad + \alpha_{nf}\left(\frac{\partial^2 \bar{T}}{\partial \bar{r}^2} + \frac{1}{\bar{r}}\frac{\partial \bar{T}}{\partial \bar{r}} + \frac{\partial^2 \bar{T}}{\partial \bar{z}^2}\right).
\end{aligned} \tag{15}$$

Dimensionless quantities that are used in the above equations are

$$\begin{aligned}
w &= \frac{\bar{w}}{c}, \quad \zeta_1 = \frac{a}{\lambda}, \quad r = \frac{\bar{r}}{a}, \quad z = \frac{\bar{z}}{\lambda}, \\
\varepsilon &= \frac{b}{a}, \quad t = \frac{c\bar{t}}{\lambda}, \quad h = \frac{\bar{h}}{a} = 1 + \varepsilon\sin(2\pi z), \\
u &= \frac{\lambda\bar{u}}{ac}, \quad \bar{\theta} = \frac{\bar{T}-T_0}{T_0}, \quad \gamma = \frac{a^2 Q_0}{T_0 k_f}, \\
R_{en} &= \frac{ac\rho_f}{\mu_f}, \quad G_r = \frac{a^2 T_0 \rho_f \alpha_f g}{c\mu_f}, \\
p &= \frac{a^2 \bar{p}}{c\lambda\mu_f}, \quad M^2 = \frac{\sigma_f}{\mu_f}B_0^2 a^2, \quad D_a = \frac{K_1}{a^2}, \\
u &= -\frac{1}{r}\frac{\partial \psi}{\partial z}, \quad w = \frac{1}{r}\frac{\partial \psi}{\partial r}.
\end{aligned} \tag{16}$$

In the above expressions G_r, $\bar{\theta}$, R_{en}, γ, ζ_1, M, D_a represents the Grashof number, dimensionless temperature, Reynolds number, dimensionless heat source parameter, wave number, Hartmann number and Darcy number, respectively. After using the lubrication approach, the continuity equation is exactly satisfied and Eqs. (13)–(15) take the form:

$$\frac{\partial p}{\partial r} = 0, \tag{17}$$

$$\begin{aligned}
\frac{\partial p}{\partial z}\frac{\mu_f}{\mu_{nf}} &= \frac{\partial^2 w}{\partial r^2} + \frac{1}{r}\frac{\partial w}{\partial r} + G_r(1-\phi+\phi\frac{(\rho\alpha)_s}{(\rho\alpha)_f})(1-\phi)^{2.5}\theta - \frac{w+1}{D_a} \\
&\quad - M^2\left(1 + \frac{3\phi(\frac{\sigma_s}{\sigma_f}-1)}{(\frac{\sigma_s}{\sigma_f}+2)-\phi(\frac{\sigma_s}{\sigma_f}-1)}\right)(1-\phi)^{2.5}(w+1),
\end{aligned} \tag{18}$$

$$\frac{\partial^2 \bar{\theta}}{\partial r^2} + \frac{1}{r}\frac{\partial \bar{\theta}}{\partial r} + \gamma\left(\frac{2k_f + k_s + (k_f - k_s)\phi}{2k_f + k_s - (k_f - k_s)2\phi}\right) = 0. \tag{19}$$

The suitable boundary conditions in the wave frame are given as

$$\begin{aligned}
\bar{\theta} + \beta\frac{\partial \bar{\theta}}{\partial r} &= 0, \quad w + \delta\frac{\mu_{nf}}{\mu_f}\frac{\partial w}{\partial r} = -1, \quad \text{at } r = h(z), \\
\frac{\partial \bar{\theta}}{\partial r} &= 0, \quad \frac{\partial w}{\partial r} = 0, \quad \text{at } r = 0,
\end{aligned} \tag{20}$$

where $\delta = \frac{\mu_f \delta_1}{a}$, $\beta = \frac{\beta_1}{a}$ are defined as the dimensionless velocity and thermal slip parameters. Dimensionless flow rate F in the laboratory frame is associated with the dimensionless flow rate q in the wave frame and defined as

$$F = q + \frac{1}{2}\left(1 + \frac{\varepsilon^2}{2}\right), \tag{21}$$

$$q = \int_0^h rw\,dr \tag{22}$$

3 Solution of the problem

Equations (18) and (19) are solved exactly by utilizing the boundary conditions given in Eq. (20). The solutions for temperature and velocity profile are as follows

Table 2 Comparison of temperature profile for different values of slip parameter β

θ	Pure blood ($\phi = 0.00$)			Copper blood			Silver blood		
r	$\beta = 0.00$	$\beta = 0.05$	$\beta = 0.09$	$\beta = 0.00$	$\beta = 0.05$	$\beta = 0.09$	$\beta = 0.00$	$\beta = 0.05$	$\beta = 0.09$
$-h$	0	0.005	0.009	0	0.00432	0.00777	0	0.00432	0.00778
-0.8	0.018	0.023	0.027	0.01555	0.01987	0.02333	0.01556	0.01988	0.02334
-0.6	0.032	0.037	0.041	0.02765	0.03197	0.03542	0.02766	0.03198	0.03543
-0.4	0.042	0.047	0.051	0.03629	0.04061	0.04406	0.03629	0.04062	0.04407
-0.2	0.048	0.053	0.057	0.04147	0.04579	0.04953	0.04148	0.04580	0.04954
0	0.05	0.055	0.059	0.04320	0.04752	0.05098	0.04321	0.04753	0.05099
0.2	0.048	0.053	0.057	0.04147	0.04579	0.04953	0.04148	0.04579	0.04954
0.4	0.042	0.047	0.051	0.03629	0.04061	0.04406	0.03629	0.04062	0.04407
0.6	0.032	0.037	0.041	0.027651	0.03197	0.03542	0.02766	0.03198	0.03543
0.8	0.018	0.023	0.027	0.015553	0.01987	0.02333	0.01556	0.01988	0.02334
h	0	0.005	0.009	0	0.00432	0.00777	0	0.00433	0.00778

$$\bar{\theta} = \gamma \left(\frac{k_s + 2k_f + \phi(k_f - k_s)}{k_s + 2k_f - 2\phi(k_f - k_s)} \right) \left(\frac{h^2 - r^2 + 2h\beta}{4} \right), \qquad (23)$$

$$\begin{aligned}
w = & \left(\frac{D_1 h^2}{S^2(I_0(Sh) + S\frac{\mu_f}{\mu_{nf}}I_1(Sh))} + \frac{4D_1}{S^4(I_0(Sh) + S\frac{\mu_f}{\mu_{nf}}I_1(Sh))} \right. \\
& \left. + \frac{2D_1 h}{S^2(I_0(Sh) + S\frac{\mu_f}{\mu_{nf}}I_1(Sh))} - \frac{1}{I_0(Sh) + S\frac{\mu_f}{\mu_{nf}}I_1(Sh)} \right) I_0(Sr) \\
& + \frac{\mu_f}{\mu_{nf}} \frac{1}{S^2(I_0(Sh) + S\frac{\mu_f}{\mu_{nf}}I_1(Sh))} \frac{dp}{dz} I_0(Sr) \\
& + \frac{(-D_1 h^2 - 2D_1 h\beta + S^2)}{S^2(I_0(Sh) + S\frac{\mu_f}{\mu_{nf}}I_1(Sh))} I_0(Sr) \\
& - \frac{D_1}{S^2} r^2 - \frac{4D_1}{S^4} + D_1 h^2 + 2D_1 h\beta \\
& - 1 - \frac{1}{S^2} \frac{\mu_f}{\mu_{nf}} \frac{dp}{dz},
\end{aligned} \qquad (24)$$

where

$$D_1 = (1 - \phi + \varphi \frac{(\rho\alpha)_s}{(\rho\alpha)_f})(1 - \phi)^{2.5} \frac{\gamma}{4} \frac{K_f}{K_{nf}},$$

$$S = \sqrt{M^2 \left(1 + \frac{3(\frac{\sigma_s}{\sigma_f} - 1)\phi}{(\frac{\sigma_s}{\sigma_f} + 2) - (\frac{\sigma_s}{\sigma_f} - 1)\phi} \right)(1 - \phi)^{2.5} + \frac{1}{Da}} \qquad (25)$$
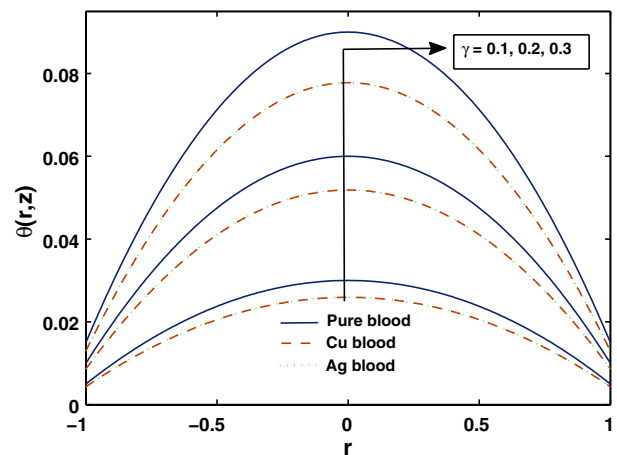
Flow rate is given as

Fig. 2 Temperature profile for various values of the heat source parameter γ

$$q = \int_0^h rw \, dr \qquad (26)$$

By substituting Eq. (24) into Eq. (26), we obtain the pressure gradient as defined below (Table 2),

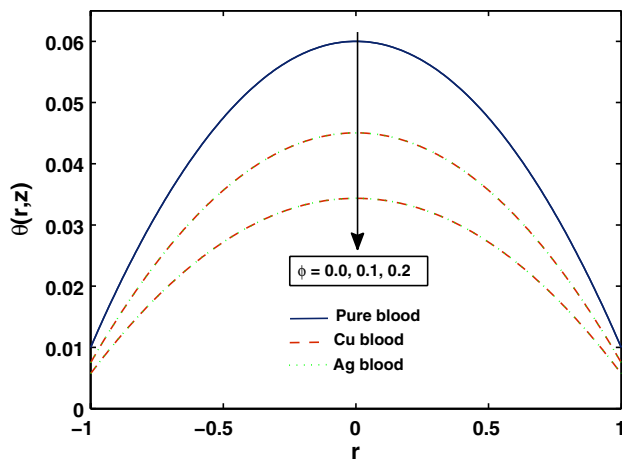$$\frac{dp}{dz} = \frac{q - l_1}{l_2} \qquad (27)$$

Fig. 3 Temperature profile for various values of the nanoparticle volume fraction ϕ
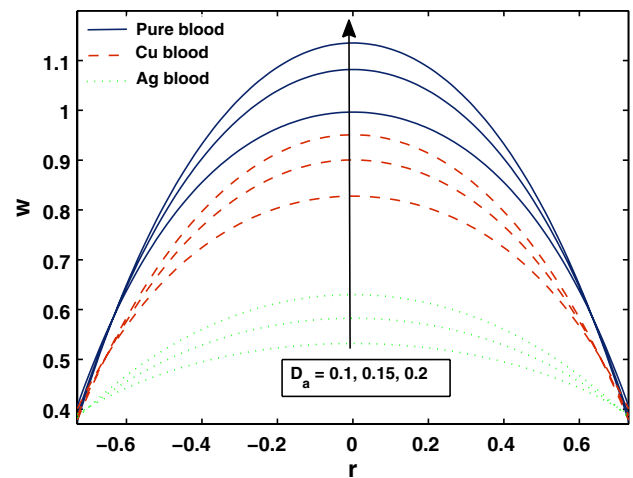

Fig. 4 Variation of velocity profile for particular values of the Darcy number D_a

where

$$
\begin{aligned}
l_1 &= \frac{\left(\frac{D_1 h^2}{S^2(I_0(Sh)+S\frac{\mu_f}{\mu_{nf}}I_1(Sh))} + \frac{4D_1}{S^4(I_0(Sh)+S\frac{\mu_f}{\mu_{nf}}I_1(Sh))} + \frac{2D_1 h}{S^2(I_0(Sh)+S\frac{\mu_f}{\mu_{nf}}I_1(Sh))} - \frac{1}{I_0(Sh)+S\frac{\mu_f}{\mu_{nf}}I_1(Sh)}\right)hI_1(Sh)}{S} \\
&+ \frac{(-D_1 h^2 - 2D_1 h\beta + S^2)hI_1(Sh)}{S^3(I_0(Sh)+S\frac{\mu_f}{\mu_{nf}}I_1(Sh))} + \left(-\frac{D_1 h^4}{4S^2} + -\frac{4D_1}{S^4} + D_1 h^2 + 2D_1 h\beta - 1\right)\frac{h^2}{2}, \\
l_2 &= \frac{\mu_f}{\mu_{nf}}\frac{hI_1(Sh)}{S^3(I_0(Sh)+S\frac{\mu_f}{\mu_{nf}}I_1(Sh))} - \frac{1}{S^2}\frac{\mu_f}{\mu_{nf}}\frac{h^2}{2}.
\end{aligned}
\tag{28}
$$

4 Graphical results and discussion

Impact of silver and copper nanoparticles with the aid of embedded parameters on the characteristics of peristaltic flow is presented in this section through the graphs of temperature, axial velocity, pressure gradient, pressure rise and stream lines. These graphs are prepared by controlling the parameters restricted such as $\phi = 0.0 - 0.2$, $\gamma = 0.1 - 0.3$, $D_a = 0.1 - 0.2$, $M = 0.1 - 1.5$, $\delta = 0.00 - 0.09$, $\beta = 0.0 - 0.2$, $G_r = 0.5 - 1.5$. Influence of different embedded parameters such as heat source (γ), and nanoparticle volume fraction (ϕ) on temperature profile is shown in Figs. 2 and 6. Significant growth in temperature is shown in Fig. 2 with increasing values of heat source parameter γ. Temperature profile decreases when the volume fraction ϕ is increased. It is depicted that the heat being gained by the heat source is rapidly transferred to the walls (due to the inclusion of nanoparticles) and thus the fluid temperature decreases (Fig. 3). Effective thermal conductivity of nanoparticles plays a key role in the quick decrease of the fluid temperature. This supports the inclusion of nanoparticles in peculiar situation such as coolants. We primarily focus to inspect

the behaviors of various embedded parameters like Darcy number (D_a), Hartmann number (M), Velocity slip parameter (δ), Thermal slip parameter (β), Heat source/sink parameter (γ) and Grashof number (G_r) on velocity profile as shown in Figs. 4, 5, 6, 7, 8 and 9. All these
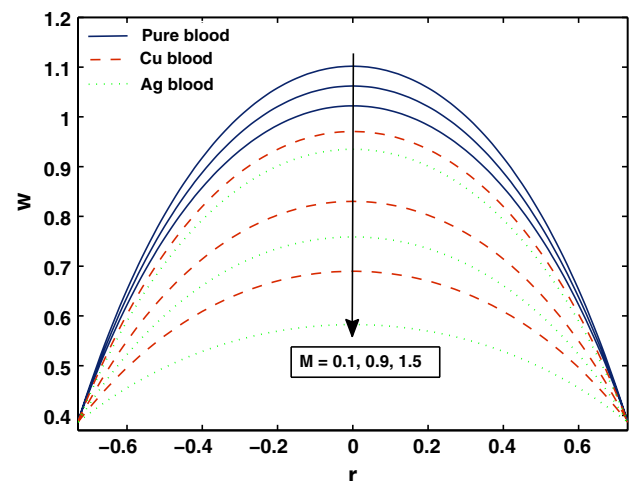

Fig. 5 Variation of velocity profile for particular values of the Hartmann number M
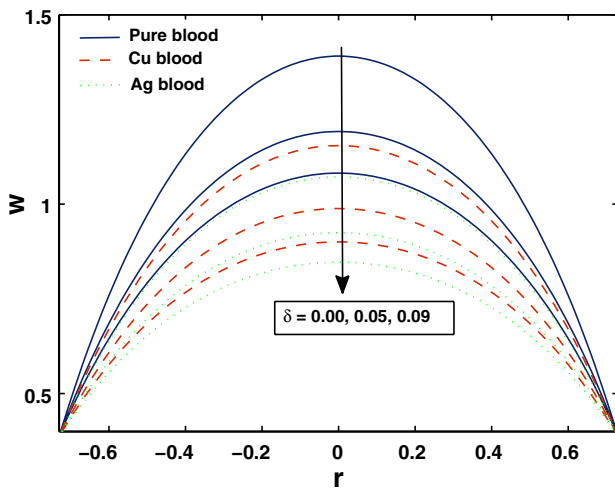
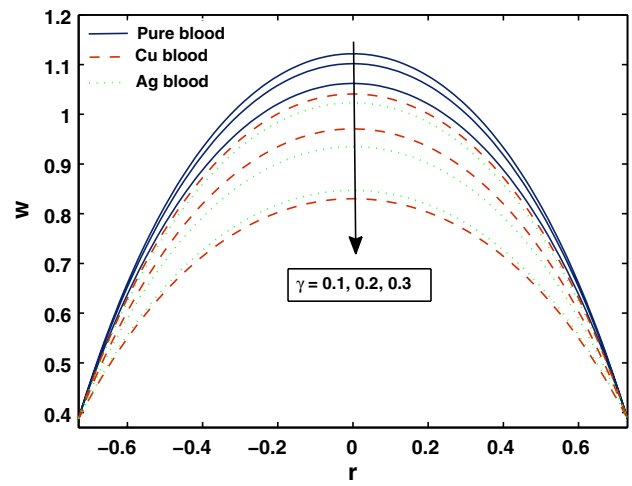**Fig. 6** Variation of velocity profile for particular values of the velocity slip parameter δ

Fig. 8 Variation of velocity profile for particular values of the heat source/sink parameter γ
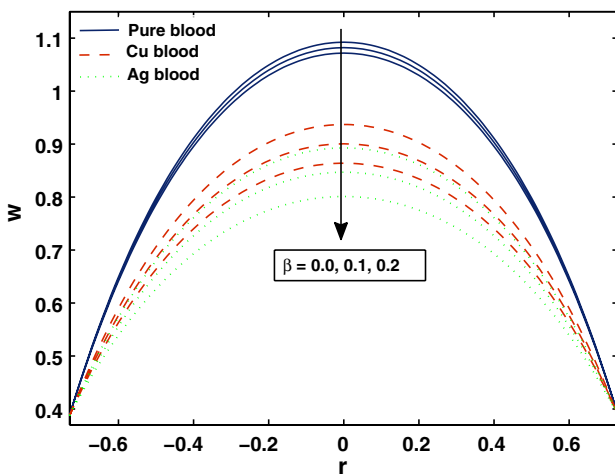

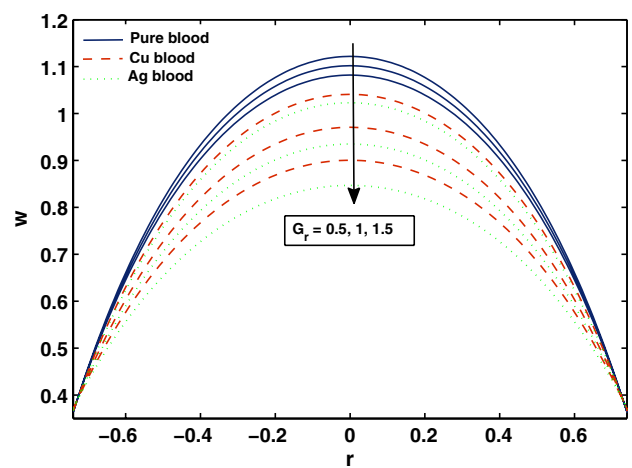**Fig. 7** Variation of velocity profile for particular values of the thermal slip parameter β

Fig. 9 Variation of velocity profile for particular values of the Grashof number G_r

figures illustrated that the velocity profile attains maximum value at the center and traces a trajectory like parabolic curve. Furthermore, maximum value of velocity is greater for pure blood when compared with copper blood and silver blood. It is also seen from these figures that the maximum velocity of base fluid reduces due to the accession of nanoparticles. Velocity profile for distinct values of Darcy number (D_a) is plotted in Fig. 4. We examine that the significance of velocity increases with the increase of the values of D_a. The effect is of sublime importance in blood capillaries where pores in walls allow exchange of water, oxygen and many other nutrients between the blood and the tissues. Figure 5 depicts that an increase in the value of Hartmann number (M) decreases the velocity around the center of the tube.

Moreover, this figure also described that the significantly strong magnetic field reduces the velocity profile of vertical tube. The mitigating aspect of MHD aids in curing and treatment of arthritis, cancer and migraine without effecting blood flow stream. Figures 6 and 7 shows the behavior for different values of the velocity slip parameter (δ) and thermal slip parameter (β). It is elucidated that the velocity profiles give higher altitude for copper when compared to silver nanoparticles and reduce by increasing velocity and thermal slip parameters. We depicted from Fig. 8 that variation in heat source parameter (γ) decreases the velocity of the nanofluid. Further, it is delineated that the incorporation of silver nanoparticles decreases the velocity profile minimal higher than that of copper nanoparticles. It is analyzed that the velocity
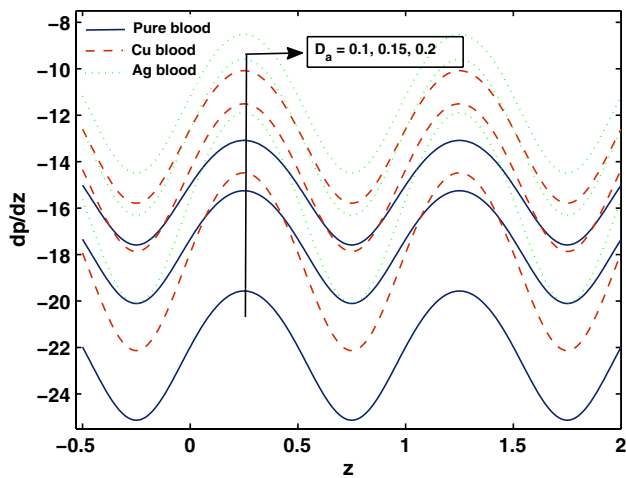
2542

J Braz. Soc. Mech. Sci. Eng. (2017) 39:2535–2560

Fig. 10 Change in pressure gradient for distant values of the Darcy number D_a
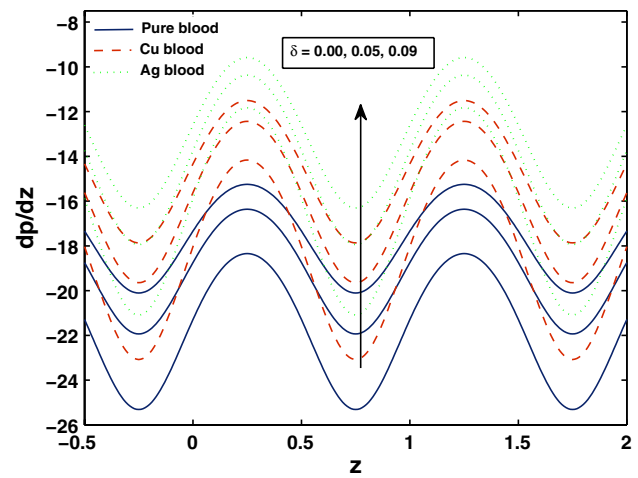

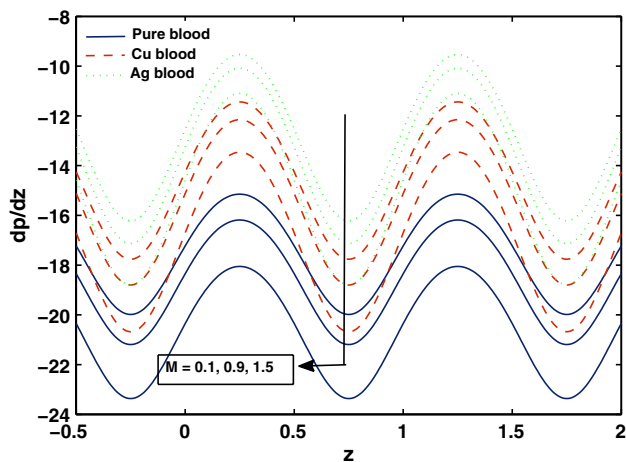**Fig. 12** Change in pressure gradient for distant values of the velocity slip parameter δ

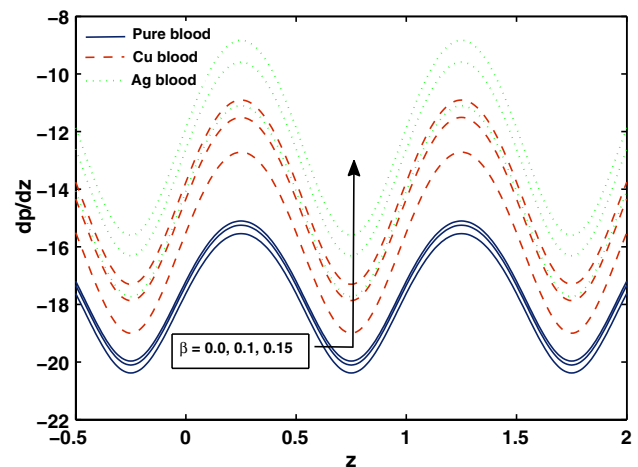**Fig. 11** Change in pressure gradient for distant values of the Hartmann number M

Fig. 13 Change in pressure gradient for distant values of the thermal slip parameter β

profile decreases with an increase in the values of Grashof number (G_r). Change in pressure gradient for Darcy number, Hartmann number, velocity slip parameter, thermal slip parameter, heat source/sink parameter and Grashof number is observed from Figs. 10, 11, 12, 13, 14, 15 and 16. Common observation from these figures is that the pressure gradient shows oscillatory behavior which is the truth be told because of peristalsis. The graph for the variation in Darcy number is described in Fig. 10 and shows that the pressure gradient enhances with the larger values of Darcy number. Note that the addition of silver nanoparticles enhances the pressure gradient slightly more than for the copper nanoparticles. Figure 11 is plotted to discuss the effects of Hartmann number M and analyze that the magnetic field decreases

the pressure gradient with increasing values of Hartmann number because magnetic field becomes stronger for higher values of Hartmann number. Figures 12 and 13 describe the effects of velocity slip parameter δ and thermal slip parameter β on the pressure gradient. It is investigated form these figures that the pressure gradient in vertical tube gives higher height for silver nanoparticles and improves on increasing thermal and velocity slip parameters. It is obtained from these figures that both the slip parameters are directly related to pressure gradient. Figure 14 depicts that the increase in heat source parameter increases the pressure gradient since more heat is generated inside the considered base fluid. The effect of Grashof number G_r on the pressure gradient is discussed in Fig. 15 and noticed that with the growth of the viscous
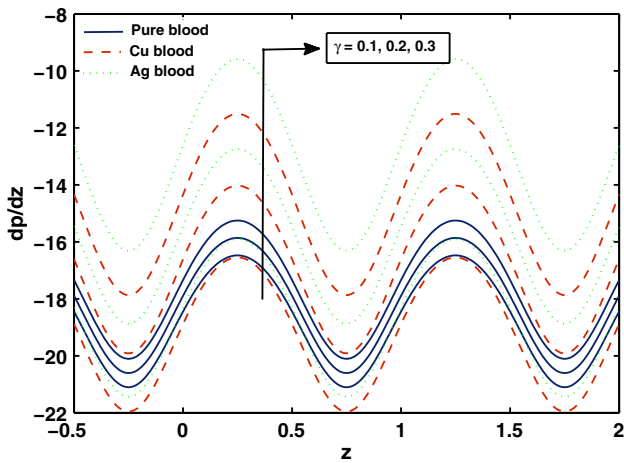
Fig. 14 Change in pressure gradient for distant values of the heat source/sink parameter γ
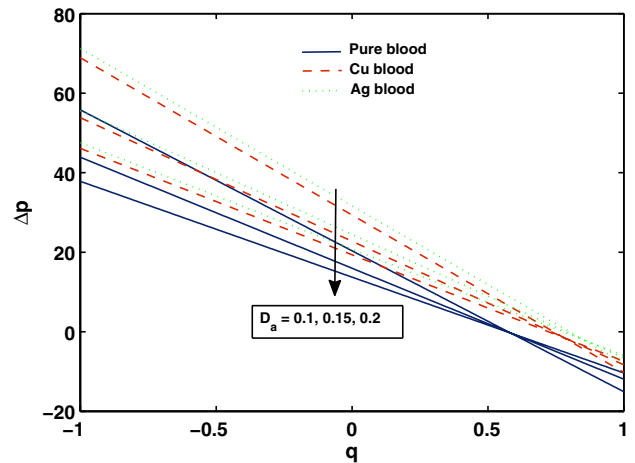

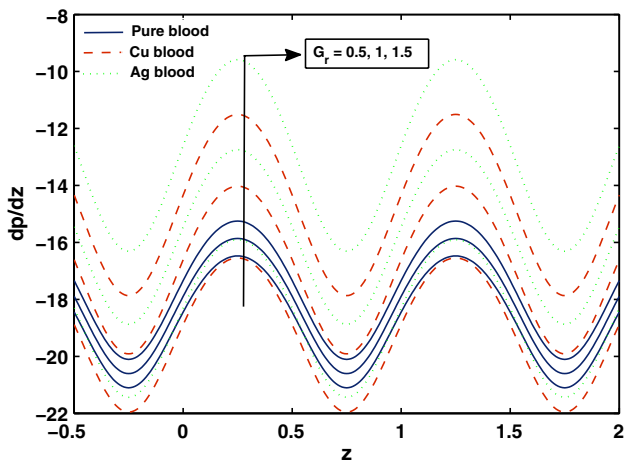**Fig. 16** Variation of pressure rise for distinct values of the Darcy number D_a

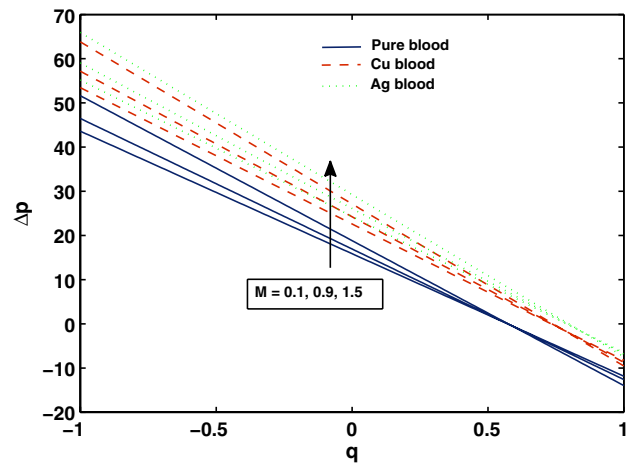**Fig. 15** Change in pressure gradient for distant values of the Grashof parameter G_r

Fig. 17 Variation of pressure rise for distinct values of the Hartmann number M

forces the pressure gradient increases. The pressure rise per wavelength is important to explain the pumping properly and sketched here from Figs. 16, 17, 18, 19, 20 and 21. One regular observation from these figures is that the pressure rise per wavelength diminishes with the expansion in flow rate. Figures 16 and 17 describe the effect of Darcy number D_a and Hartmann number M on the pressure rise. It is declared from these figures that the pressure rise per wavelength is inversely related to the Darcy number D_a and directly related to the Hartmann number M. Figures 16 and 17 enclose that inclusion of nanoparticles reduces the free pumping flux (value of q for $\Delta p = 0$). Furthermore, pressure rise upgraded in the retrograde pumping region ($q < 0$, $\Delta p > 0$) with the increase of nanoparticle volume

fraction. Figure 18 is plotted for different values of velocity slip parameter like ($\delta = 0, 0.05, 0.09$) cross ponds to no slip and slip effects, respectively. It is depicted that pressure rise declines when we consider the slip effects. The fluctuation of pressure rise versus q for different values of thermal slip parameter is given in Fig. 19 and observed that the pressure rise for the vertical tube enhances when thermal slip effects are taken into account. Figures 20 and 21 show the behavior for various values of heat source parameter and Grashof number. It is depicted from Fig. 20 that the pressure starts increasing for larger values of heat source parameter. Figure 21 shows that the pressure rise increases with an increase in the viscous forces for distinct values of Grashof number. A stream line describes a fascinating
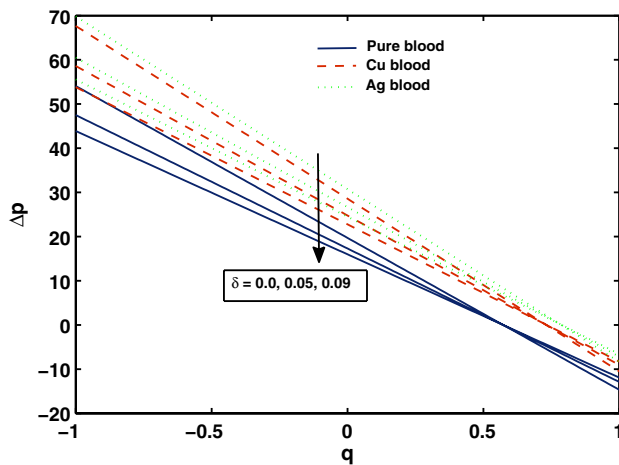
2544

J Braz. Soc. Mech. Sci. Eng. (2017) 39:2535–2560

Fig. 18 Variation of pressure rise for distinct values of the velocity slip parameter δ
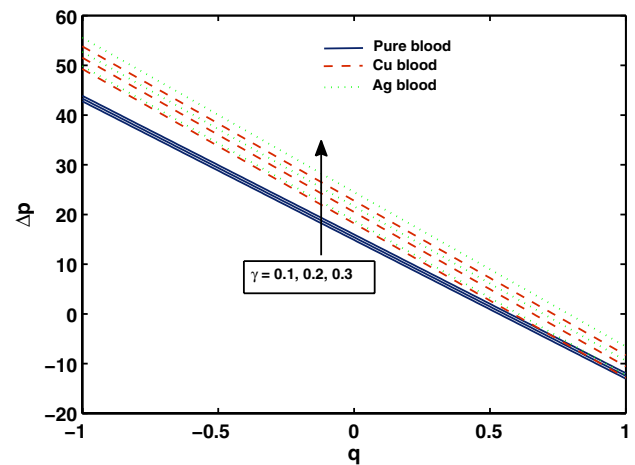

Fig. 20 Variation of pressure rise for distinct values of the heat source/sink parameter γ
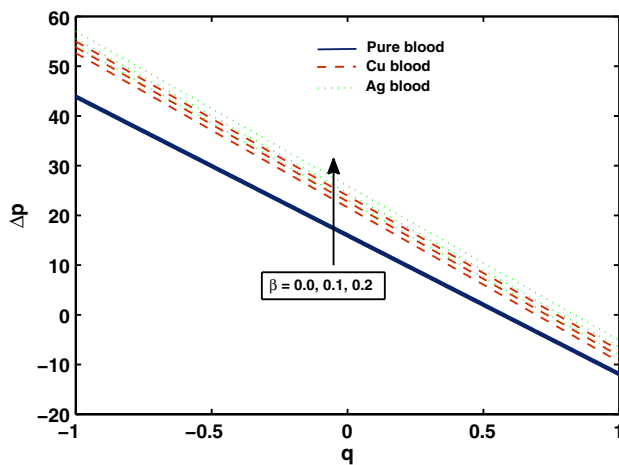

Fig. 19 Variation of pressure rise for distinct values of the thermal slip parameter β
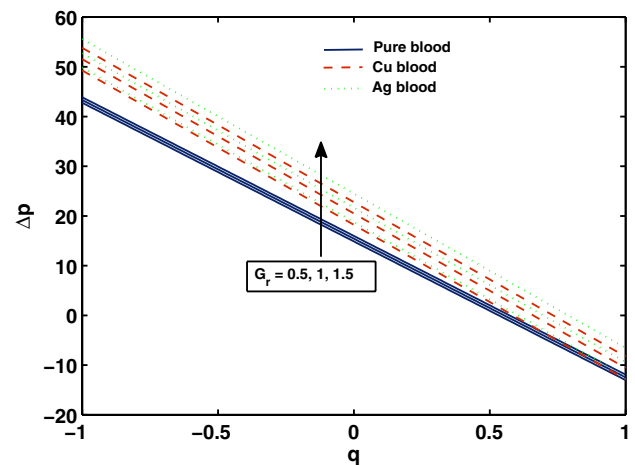

Fig. 21 Variation of pressure rise for distinct values of the Grashof number G_r

phenomenon for fluid flow of an inside flowing bolus and has been plotted here in Figs. 22, 23, 24, 25, 26, 27, 28, 29, 30, 31, 32, 33, 34 and 35 for copper and silver nanoparticles. It is analyzed that the number of trapping bolus increases by increasing Darcy number for both cases by the closed stream lines as shown in Figs. 22 and 23 . The influence of Hartmann number H_a is given in Figs. 24 and 25. It is seen that the expanding values of Hartmann number reduce the size of trapped bolus for the silver nanoparticles and enhances the trapping. The trapping phenomena for the velocity δ and thermal β slip parameters are examined through Figs. 26, 27, 28 and 29. It is inspected that more bolus appears for larger values of slip parameters when compared with no slip

effects ($\delta = 0$, $\beta = 0$). These stream lines additionally pronounce that the number of trapped bolus increases with the growth of thermal slip parameter while decreases for velocity slip parameter. The trapping phenomenon for the heat source parameter γ is given in Figs. 30 and 31. The number of the bolus increases by increasing γ for both the cases. Figures 32 and 33 are for distant values of Grashof number. We can watch from these streamlines pattern that number of bolus decreases for silver nanoparticles and size of the bolus decreases for copper nanoparticles. From Figs. 34 and 35, it is inspected that the number of trapping bolus increases when we increase the concentration of nanoparticles as contrast to pure blood case.
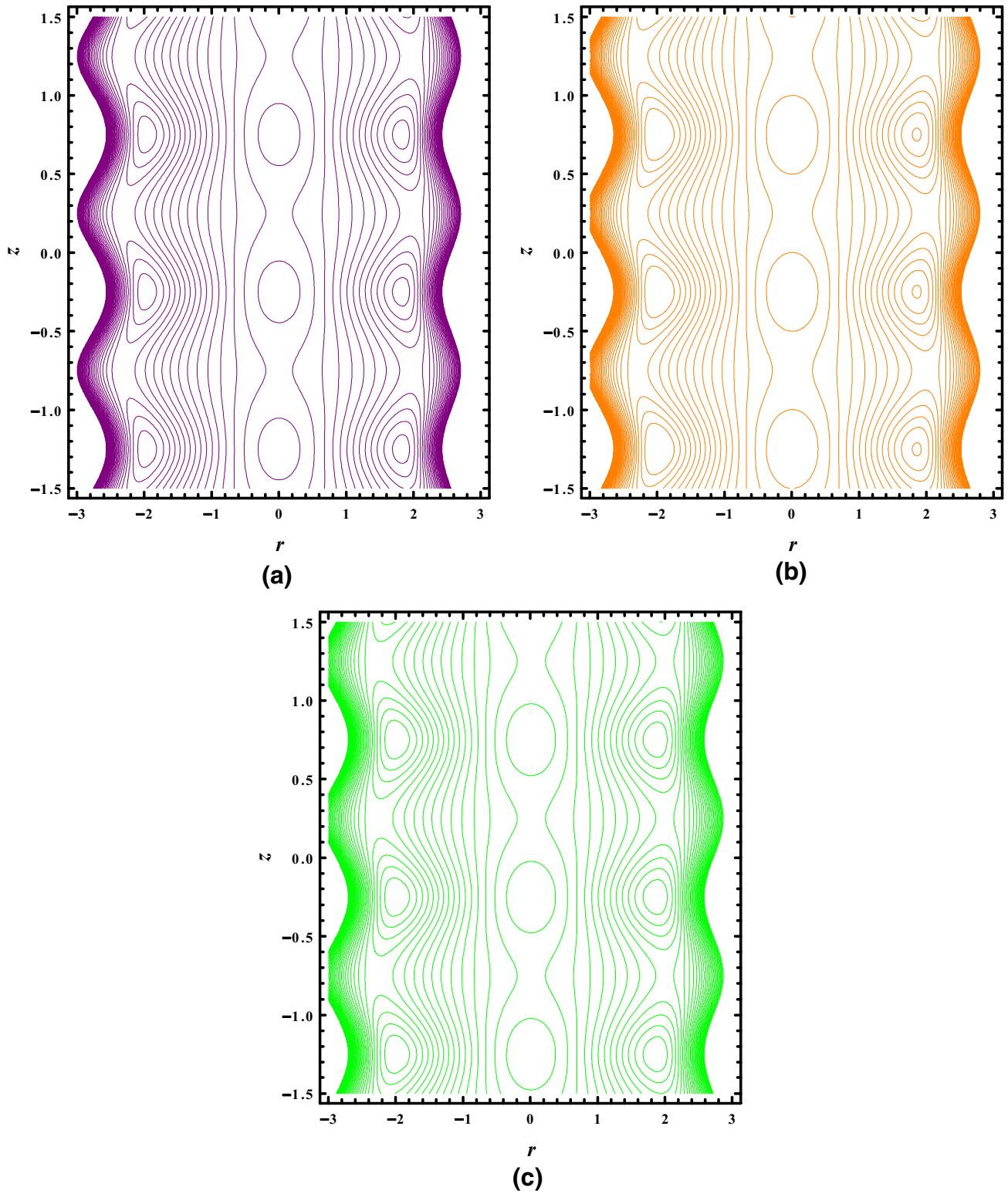
J Braz. Soc. Mech. Sci. Eng. (2017) 39:2535–2560

2545

Fig. 22 Streamlines (copper nanoparticles) for different values of the **a** $D_a = 0.1$, **b** $D_a = 0.15$, **c** $D_a = 0.2$

2546

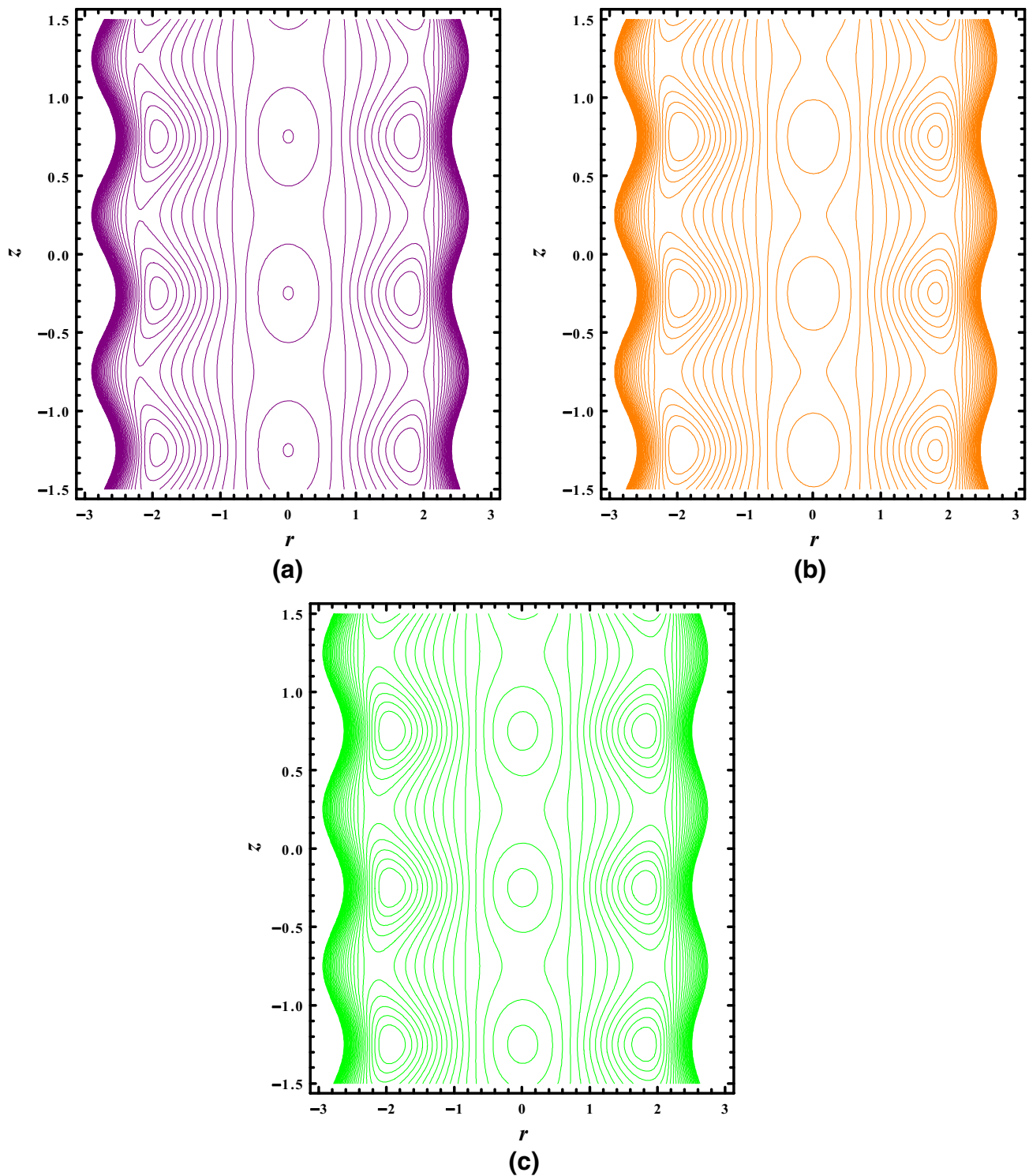J Braz. Soc. Mech. Sci. Eng. (2017) 39:2535–2560

Fig. 23 Streamlines (silver nanoparticles) for different values of the **a** $D_a = 0.1$, **b** $D_a = 0.15$, **c** $D_a = 0.2$

5 Conclusions

In this investigation, we have analyzed the impinging of silver and copper nanoparticles on MHD flow along slip effects through a porous medium. The impact of different rheological parameters on the important flow quantities is described via graphs. Some crucial observations of the present analysis are mentioned as,
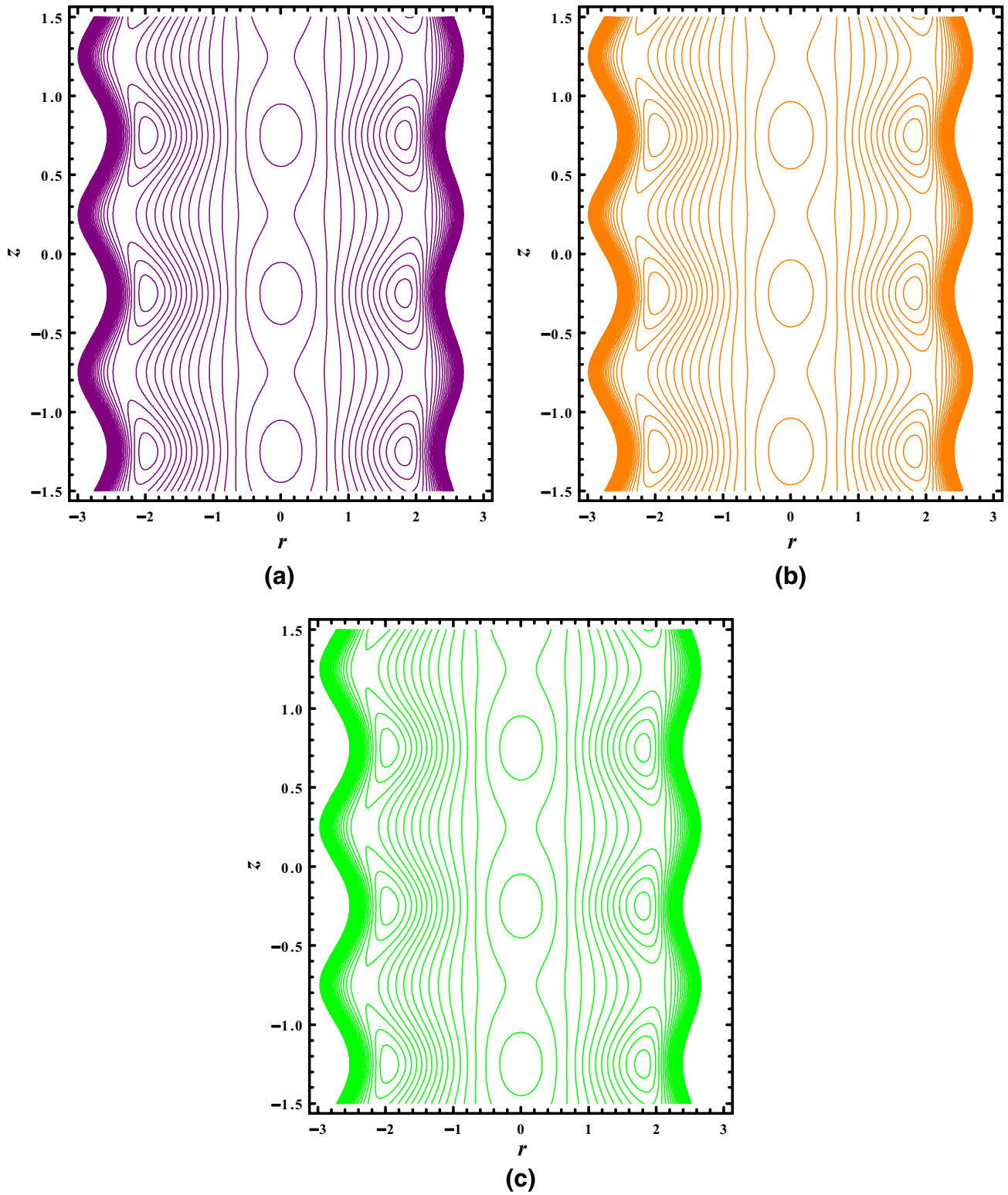
Fig. 24 Streamlines (copper nanoparticles) for different values of the **a** $M = 0.05$, **b** $M = 0.1$, **c** $M = 0.2$
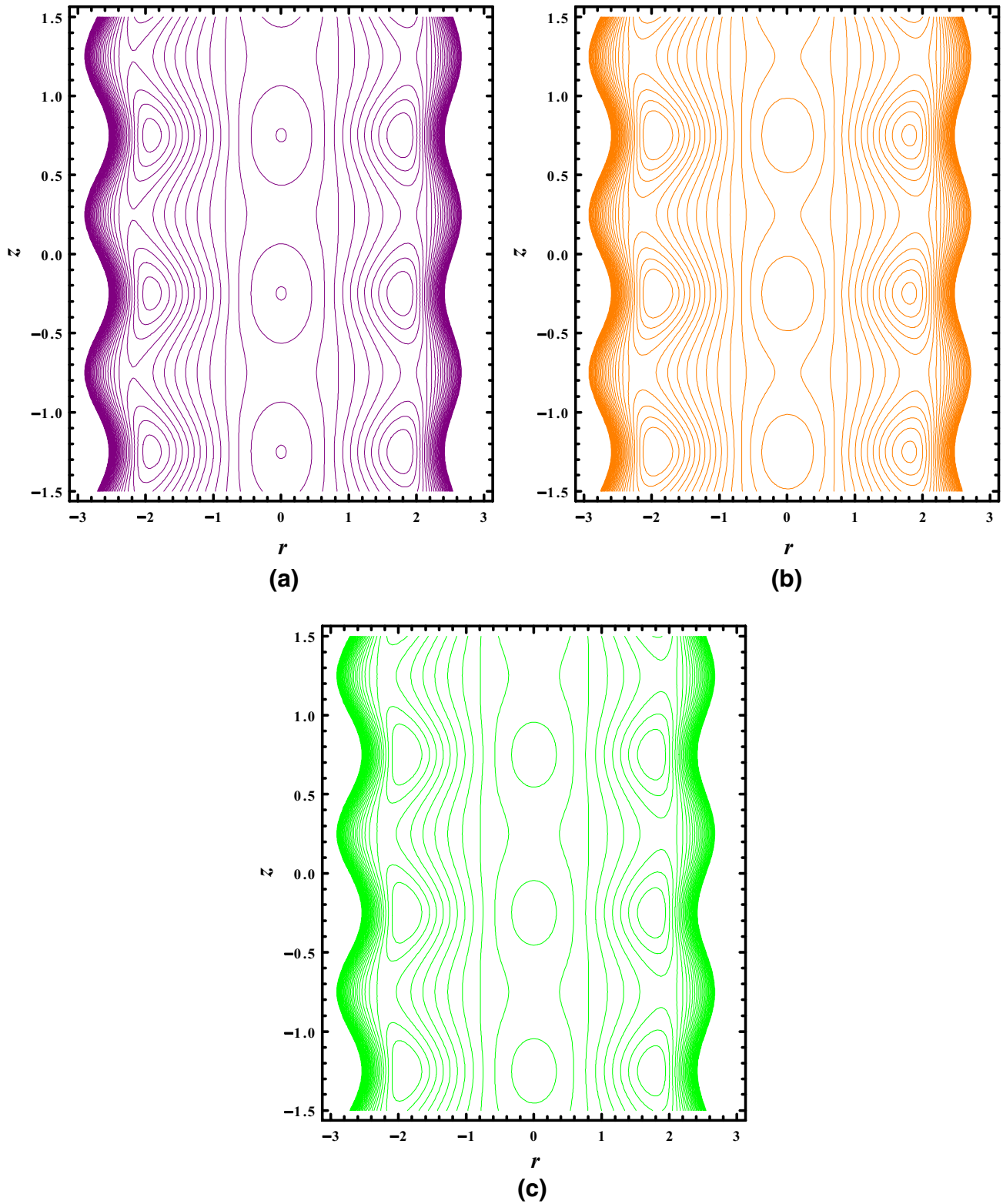
2548

J Braz. Soc. Mech. Sci. Eng. (2017) 39:2535–2560

Fig. 25 Streamlines (silver nanoparticles) for different values of the **a** $M = 0.05$, **b** $M = 0.1$, **c** $M = 0.2$
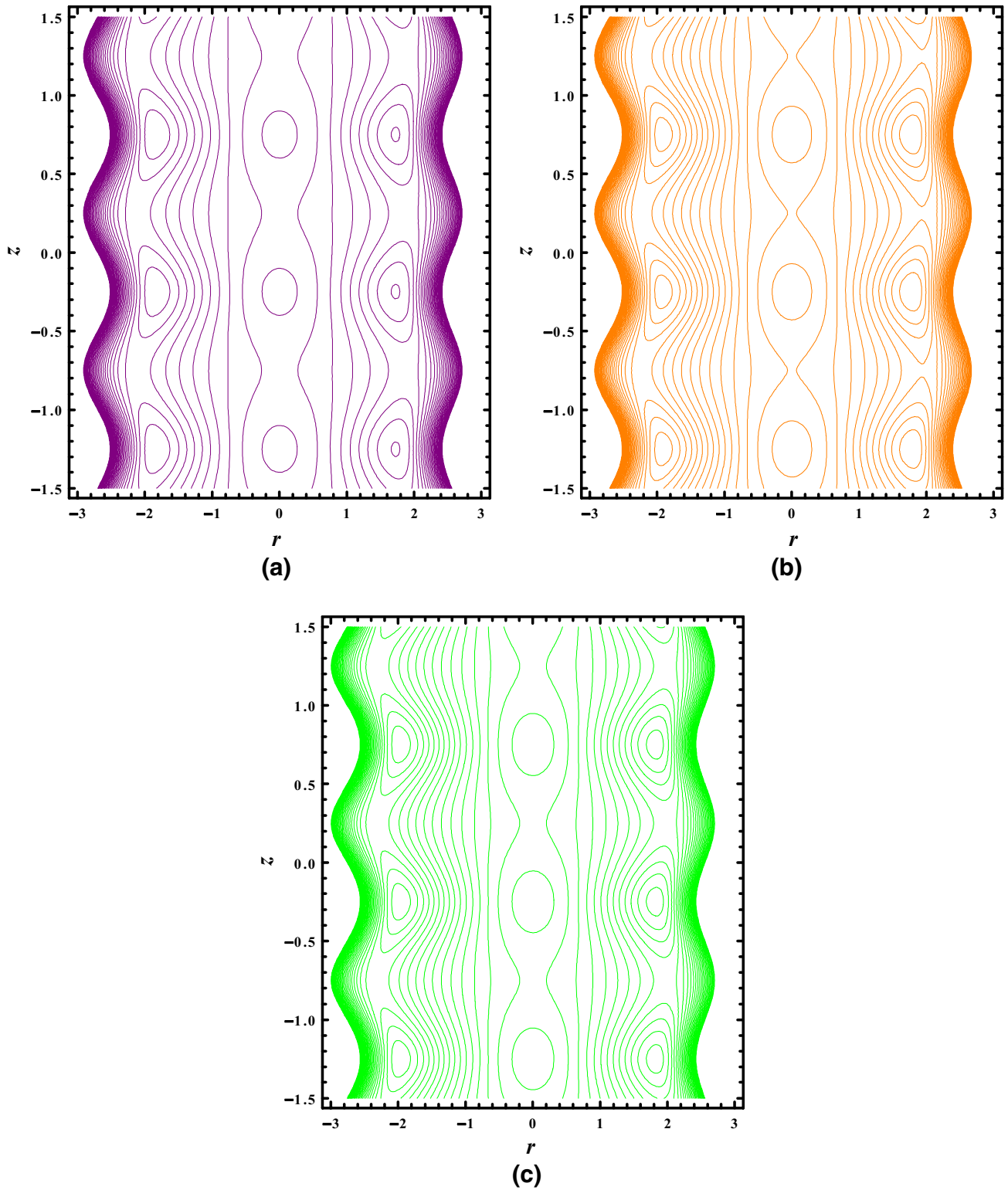
Fig. 26 Streamlines (copper nanoparticles) for different values of the **a** $\delta = 0.00$, **b** $\delta = 0.05$, **c** $\delta = 0.09$

2550

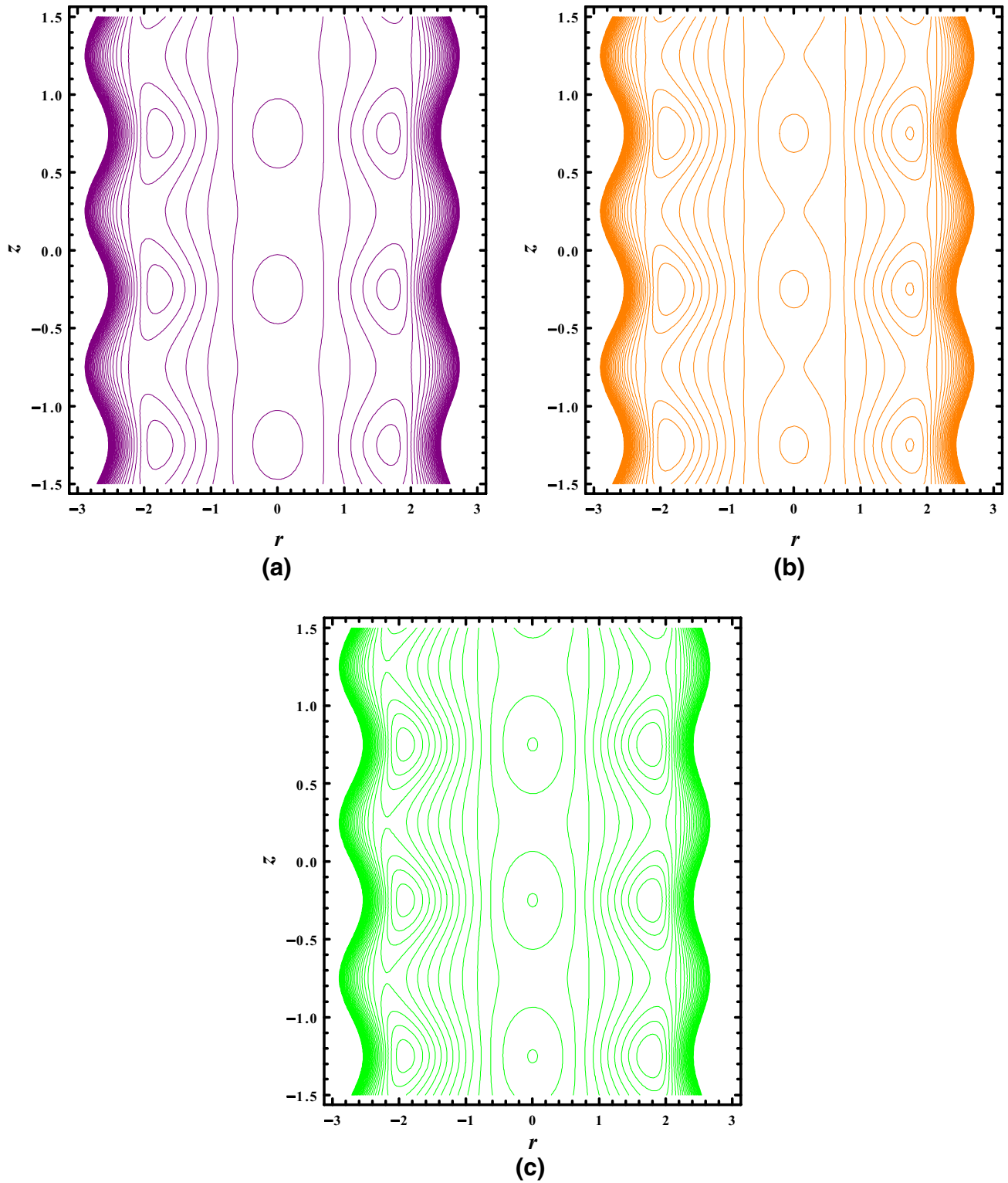J Braz. Soc. Mech. Sci. Eng. (2017) 39:2535–2560

Fig. 27 Streamlines (silver nanoparticles) for different values of the **a** $\delta = 0.00$, **b** $\delta = 0.05$, **c** $\delta = 0.09$
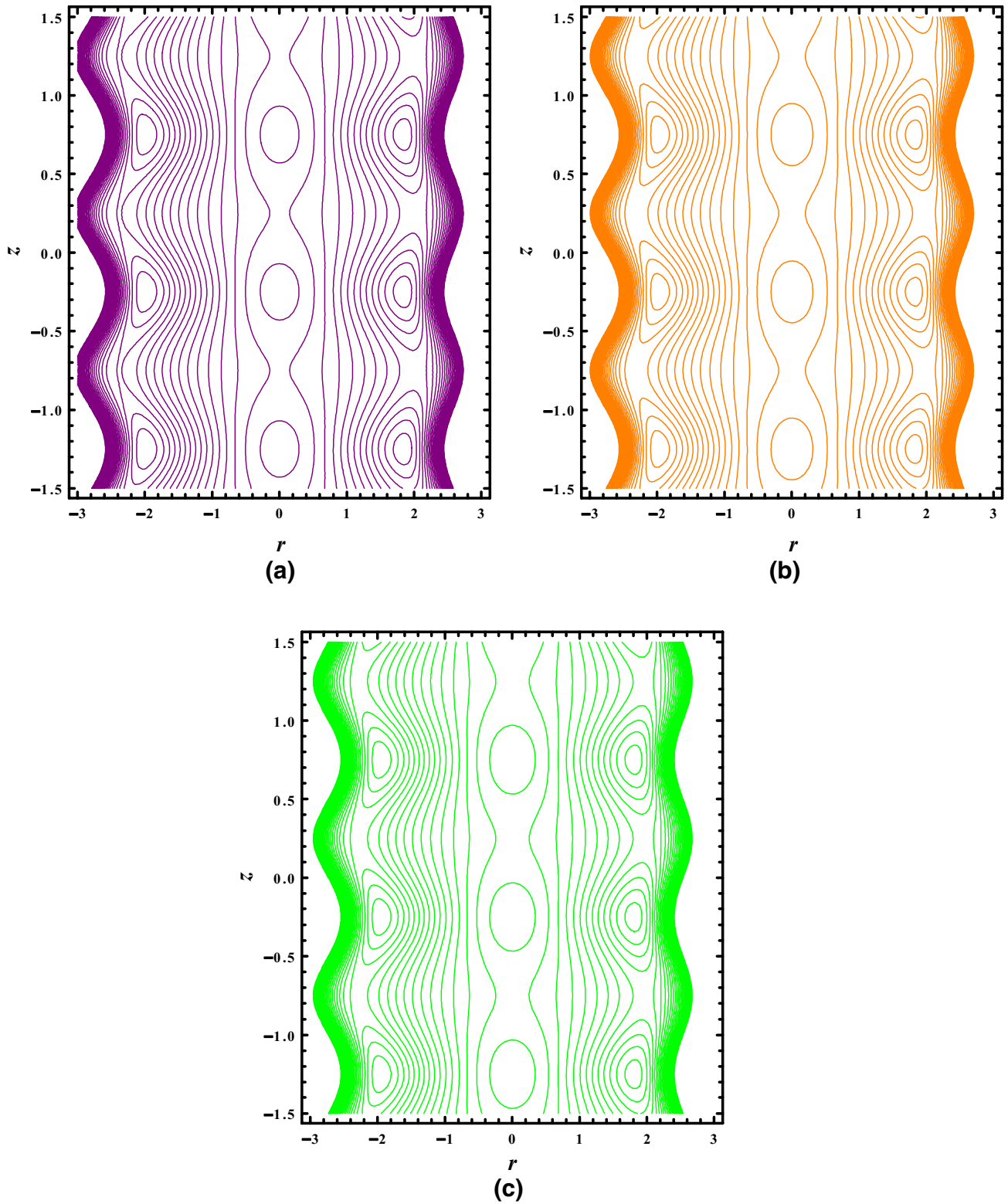
Fig. 28 Streamlines (copper nanoparticles) for different values of the **a** $\beta = 0.00$, **b** $\beta = 0.05$, **c** $\beta = 0.09$
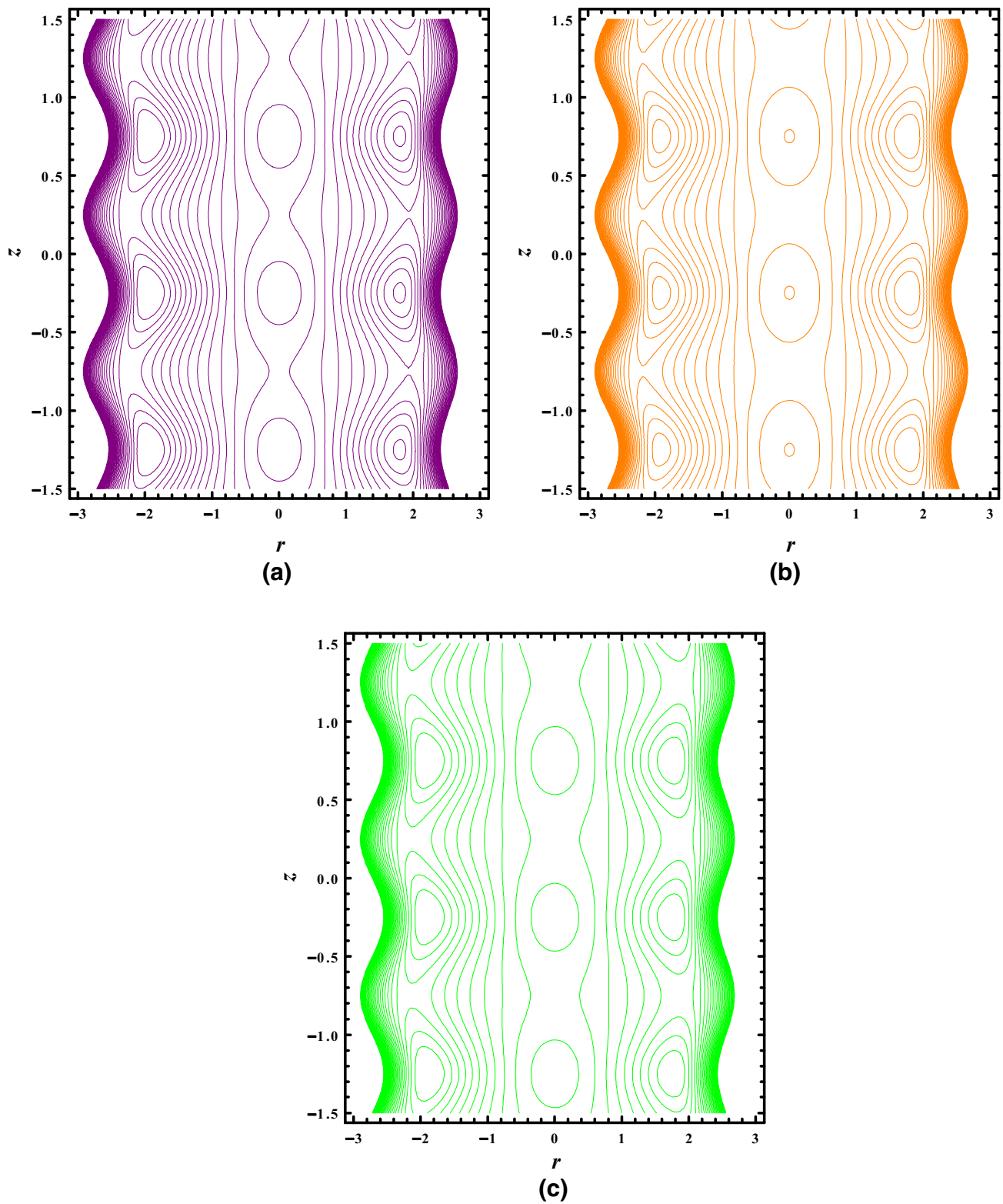
Fig. 29 Streamlines (silver nanoparticles) for different values of the **a** $\beta = 0.00$, **b** $\beta = 0.05$, **c** $\beta = 0.09$
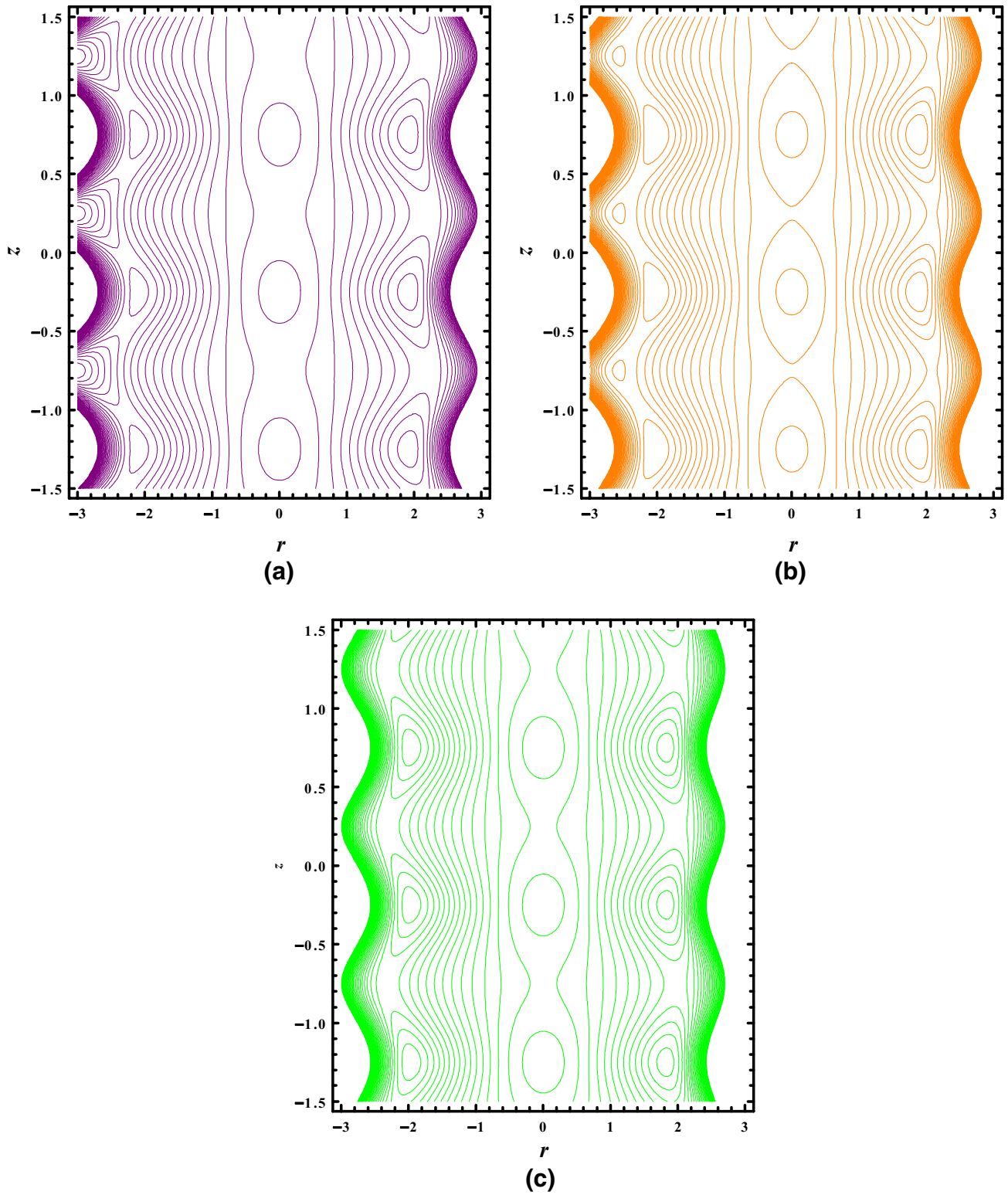
Fig. 30 Streamlines (copper nanoparticles) for different values of the **a** $\gamma = 0.1$, **b** $\gamma = 0.2$, **c** $\gamma = 0.3$
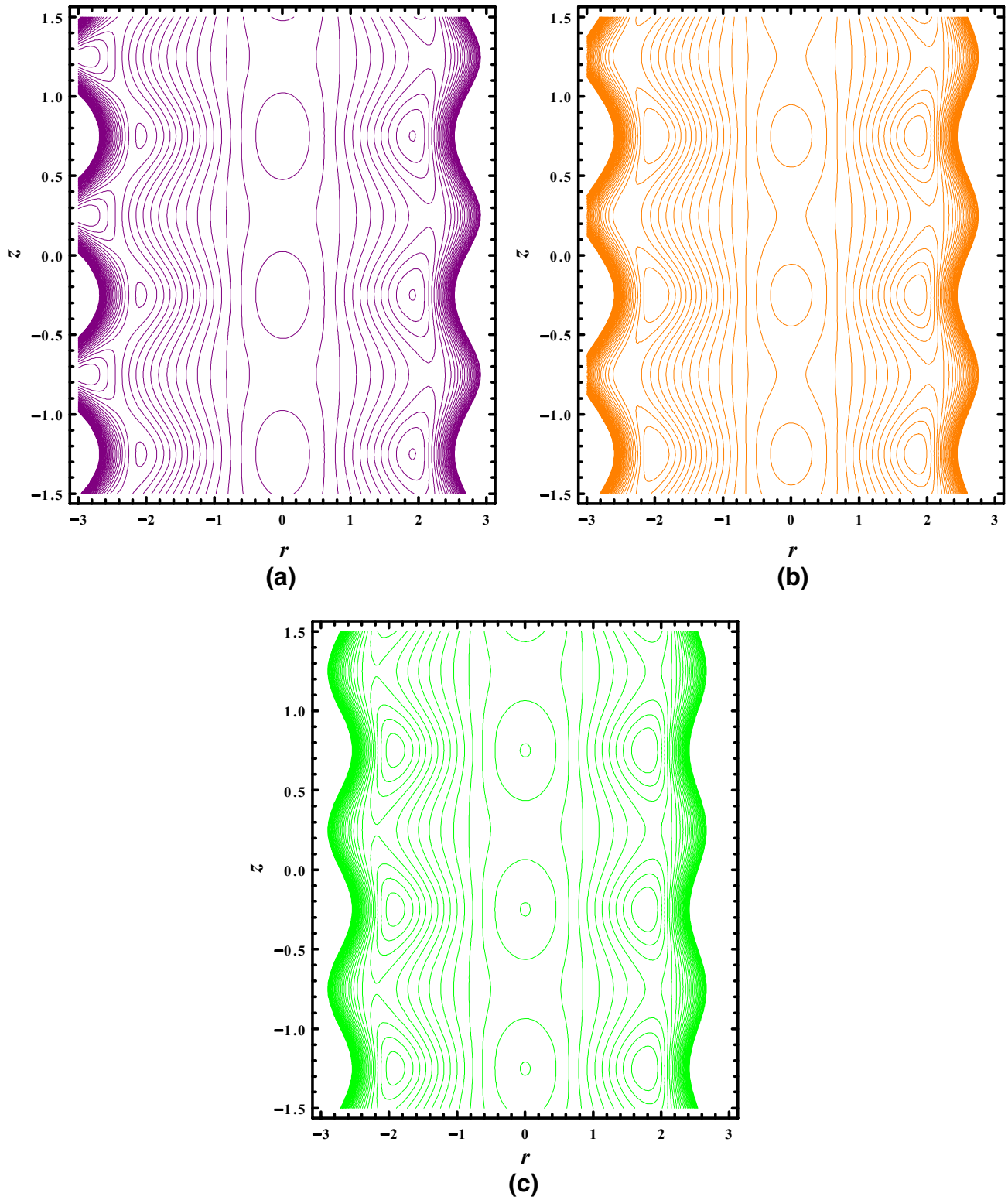
2554

J Braz. Soc. Mech. Sci. Eng. (2017) 39:2535–2560

Fig. 31 Streamlines (silver nanoparticles) for different values of the **a** $\gamma = 0.1$, **b** $\gamma = 0.2$, **c** $\gamma = 0.3$

Fig. 32 Streamlines (copper nanoparticles) for different values of the **a** $G_r = 1$, **b** $G_r = 1.3$, **c** $G_r = 1.6$

2556

J Braz. Soc. Mech. Sci. Eng. (2017) 39:2535–2560

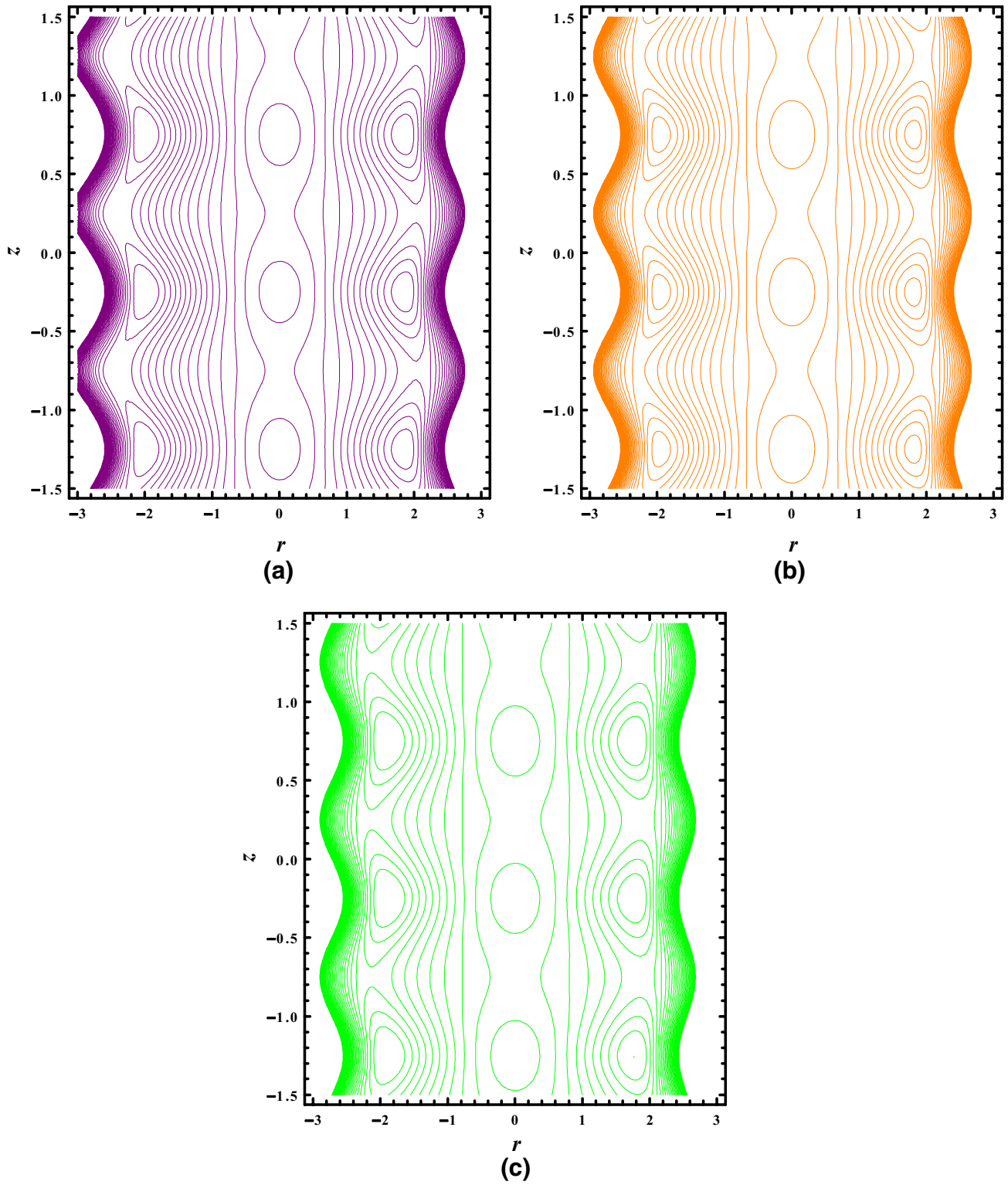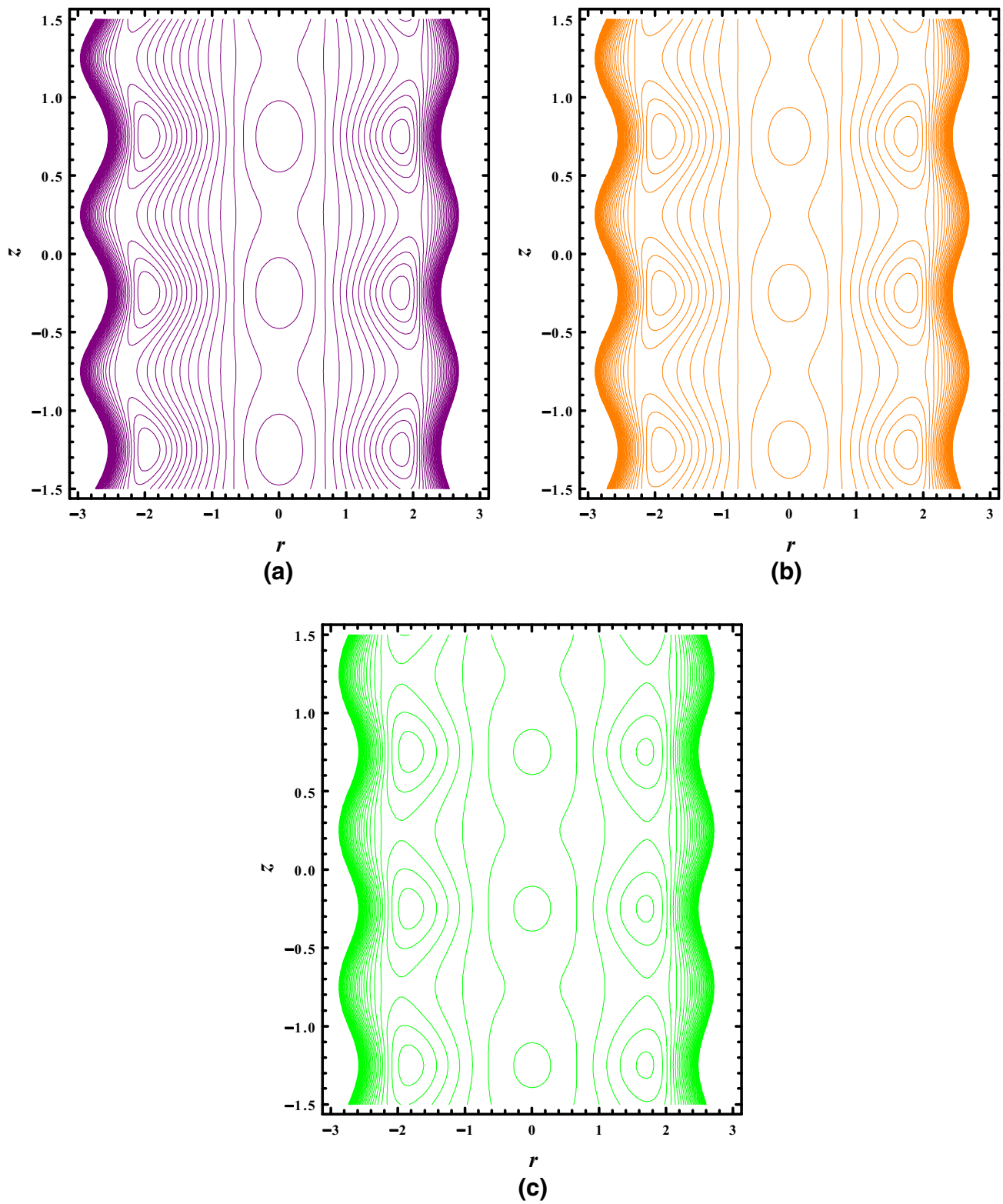**Fig. 33** Streamlines (silver nanoparticles) for different values of the **a** $G_r = 1$, **b** $G_r = 1.3$, **c** $G_r = 1.6$

J Braz. Soc. Mech. Sci. Eng. (2017) 39:2535–2560

2557

Fig. 34 Streamlines (copper nanoparticles) for different values of the **a** $\phi = 0.00$ (pure blood), **b** $\phi = 0.05$, **c** $\phi = 0.09$
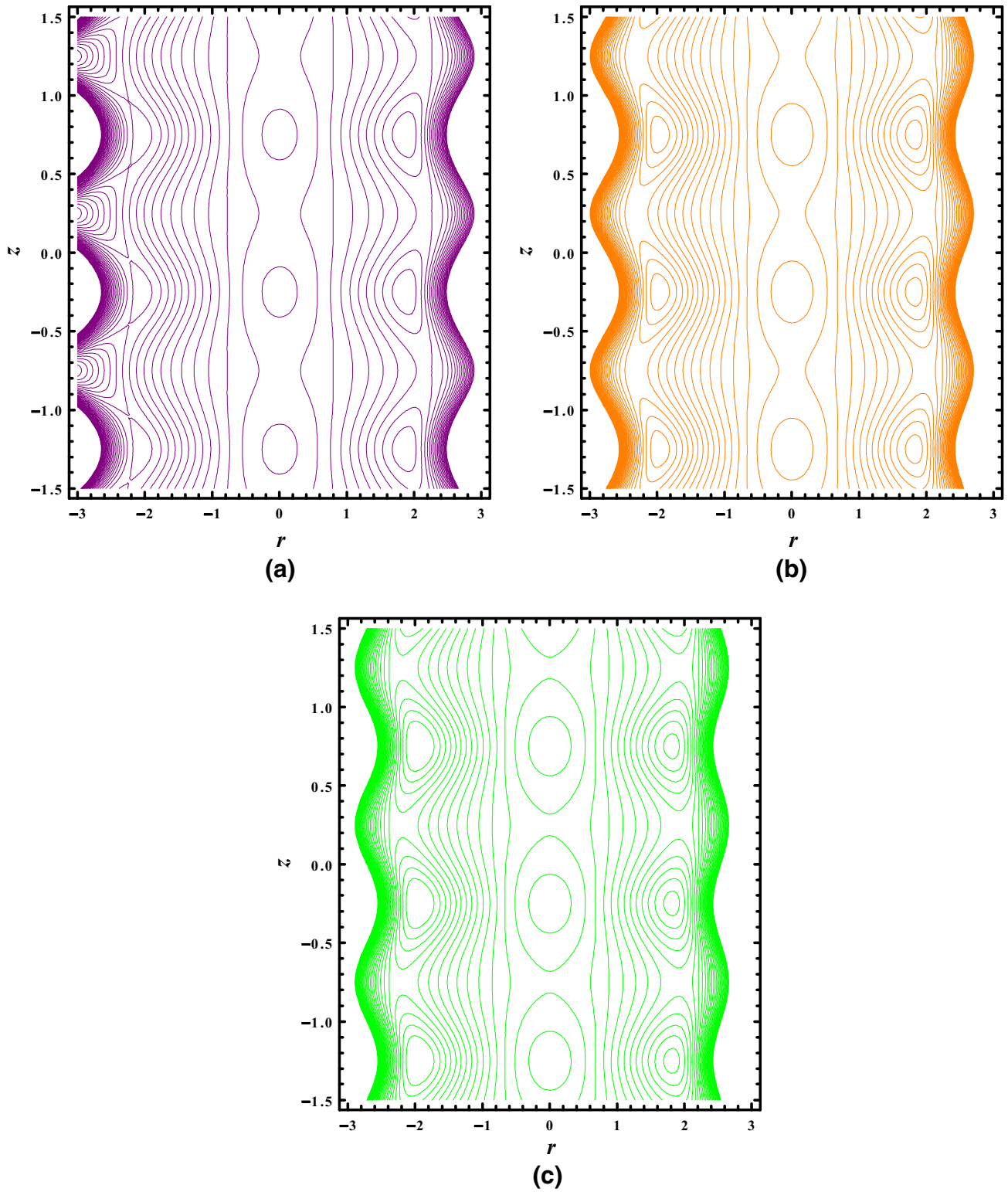
2558

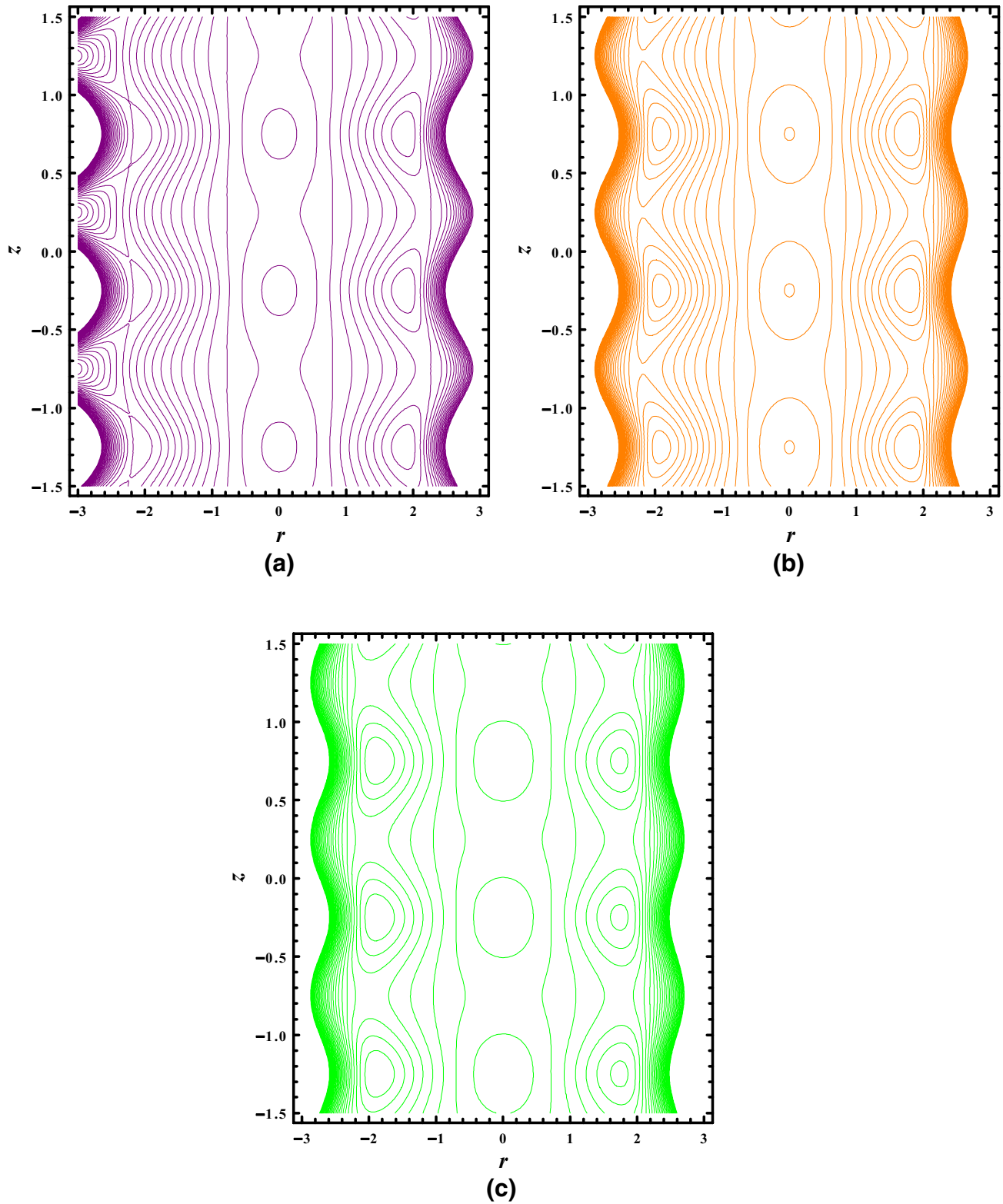J Braz. Soc. Mech. Sci. Eng. (2017) 39:2535–2560

Fig. 35 Streamlines (silver nanoparticles) for different values of the **a** $\phi = 0.00$ (pure blood), **b** $\phi = 0.05$, **c** $\phi = 0.09$

- It is noted that the temperature inside the vertical tube increases for heat source parameter ($\gamma > 0$). This result is obtained due to increase in internal heat source of the fluid, i.e., through metabolic process.
- With the increase of nanoparticle volume fraction, temperature of the nanofluid decreases with an increase in the nanoparticle volume fraction because high thermal conductivity of nanoparticles plays a key role in quick dissipation of the temperature. This observation justifies the use of nanoparticles as coolants in several engineering applications
- Velocity profiles exhibit higher results for pure blood than for the copper blood and silver blood.
- It is observed with an increase in the intensity of magnetic field velocity profile decreases. This result is concluded from the fact that the external magnetic field slows down the random motion of nanoparticles and hence also tends down the blood movement.
- It is elucidated that the velocity increases for velocity and thermal slip parameters which is physically true because slip effects reduce the drag force between the boundary and fluid and hence velocity increases.
- Pressure gradient increases with increasing nanoparticle volume fraction. It is due to the fact that the inclusion of nanoparticles allows the quick passage of fluid through vertical tube.
- Pressure rise enhances due to the impulsion of metallic nanoparticles when compared to that of the pure blood ($\phi = 0.00$).
- The number of bolus increases throughout the vertical tube with the addition of silver and copper nanoparticles in the presence of slip effects when compare with ($\beta = 0, \delta = 0$).
- The trapping bolus phenomenon shows that the number of the bolus increases with an increase in the concentration of nanoparticles as compared to the pure blood case ($\phi = 0$).

References

1. Shapiro AH, Jaffrin MY, Wienberg S (1969) Peristaltic pumping with long wavelengths at low Reynolds number. J Fluid Mech. 37:799–825
2. Srivastava LM, Srivastava VP, Sinha SN (1983) Peristaltic transport of a physiological fluid. Part I. Flow in non-uniform geometry. Biorheology 20:153–166
3. Rao AR, Mishra M (2004) Nonlinear and curvature effects on the peristaltic flow of a viscous fluid in an asymmetric channel. Acta Mech 168:35–59
4. Mekheimer KhS, Husseny SZA, Abdellateef AI (2011) Effect of lateral walls on peristaltic flow through an asymmetric rectangular duct. Appl Bion Biomech 8:1–14
5. Mekheimer KhS, El Shehawey EF, Elaw AM (1998) Peristaltic motion of a particle-fluid suspension in a planar channel. Int J Theor Phys 37:2896–2919
6. Abdelsalam SI, Vafai K (2017) Particulate suspension effect on peristaltically induced unsteady pulsatile flow in a narrow artery: blood flow model. Math Biosci 283:91–105
7. Ealshahed M, Haroun MH (2005) Peristaltic transport of Johnson–Segalman fluid under effect of a magnetic field. Math Probl Eng 6:663–667
8. Mekheimer KS, Elmaboud YA (2008) The influence of heat transfer and magnetic field on peristaltic transport of a Newtonian fluid in a vertical annulus: application of an endoscope. Phys Lett A 372:1657
9. Mekheimer KhS (2008) Peristaltic flow of a magneto-micropolar fluid: effect of Induced magnetic field. J Appl Math 2008:23
10. Mekheimera KS, Komyc SR, Abdelsalamd SI (2013) Simultaneous effects of magnetic field and space porosity on compressible Maxwell fluid transport induced by a surface acoustic wave in a microchannel. Chin Phys B 22:124702–12479
11. Kothandapani M, Srinivas S (2008) Non-linear peristaltic transport of a Newtonian fluid in an inclined asymmetric channel through a porous medium. Phys Lett A 372:1265–1276
12. Ellahi R, Riaz A, Nadeem S, Ali M (2012) Peristaltic flow of Carreau fluid in a rectangular duct through a porous medium. Math Probl Eng 2012:24
13. Mekheimer KS, Elmaboud YA (2008) Peristaltic flow through a porous medium in an annulus: application of an endoscope. Appl Math Inf Sci 2:103
14. El Koumy SR, El Sayed IB, Abdelsalam SI (2012) Hall and porous boundaries effects on peristaltic transport through porous medium of a Maxwell model. Transp Porous Med 94:643–658
15. Rapits A, Kafousias N, Massalas C (1982) Free convection and mass transfer flow through a porous medium bounded by an infinite vertical porous plate with constant heat flux. Z Angew Math Mech 62:489–491
16. Varshney CL (1979) The fluctuating flow of a viscous fluid through a porous medium bounded by a porous and horizontal surface. Indian J Pure Appl Math 10:1558–1572
17. Mekheimer KhS (2003) Non-linear peristaltic transport through a porous medium in an inclined planar channel. J Porous Medium 6:189–201
18. Vasudev C, Rao UR, Rao GP, Reddy MVS (2011) Peristaltic flow of a Newtonian fluid through a porous medium in a vertical tube under the effect of a magnetic field. Int J Cur Sci Res 3:105–110
19. Yin RX, Yang DZ, Wu JZ (2014) Nanoparticle drug and gene-eluting stents for the prevention and treatment of coronary restenosis. Theranostics 4:175–200
20. Godin B, Sakamoto JH, Serda RE, Grattoni A, Bouamrani A, Ferrari M (2010) Emerging applications of nanomedicine for the diagnosis and treatment of cardiovascular diseases. Trends Pharmacol Sci 31:199–205
21. Xuan Y (2003) Investigation on convective heat transfer and flow features of nanofluids. ASME J Heat Transf 125:151–155
22. Brinkman HC (1952) The viscosity of concentrated suspensions and solutions. J Chem Phys 20:571–581
23. Tiwari RK, Das MK (2007) Heat transfer augmentation in a two-sided liddriven differentially heated square cavity utilizing nanofluids. Int J Heat Mass Transf 50:2002–2018
24. Choi SUS, Eastman JA (1995) Enhancing thermal conductivity of fluids with nanoparticles. ASME Int Mech Eng Congr Expos 66:99–105
25. Buongiorono J (2006) Convective transport in nanofluids. ASME J Heat Transf 128:240–250
26. Akbar NS (2014) Metallic nanoparticles analysis for the peristaltic flow in an asymmetric channel with MHD. IEEE Trans Nanotechnol 13:357–361

27. Nadeem S, Shahzadi I (2015) Mathematical analysis for peristaltic flowof two phase nanofluid in a curved channel. Commun Theor Phys 64:547–554

28. Nadeem S, Ijaz S (2016) Impulsion of nanoparticles as a drug carrier for the theoretical investigation of stenosed arteries with induced magnetic effects. J Magn Magn Mater 410:230–241

29. Murshed SMS, Castro CAN, Lourenco MJV, Lopes MLM, Santos FJV (2011) A review of boiling and convective heat transfer with nanofluids. Renew Sustain Energ Rev 15:2342–2354

30. Akbar NS, Butt AW (2016) Bio mathematical venture for the metallic nanoparticles due to ciliary motion. Comput Methods Progr. Biomed 134:43–51

31. Nadeem S, Ijaz S (2016) Examination of nanoparticles as a drug carrier on blood flow through catheterized composite stenosed artery with permeable walls. Comput Methods Progr Biomed 133:83–94

32. Jiang Y, Reynolds C, Xiao C, Feng W, Zhou Z, Rodriguez W, Tyagi SC, Eaton JW, Saari JT, Kang YJ (2007) Dietary copper supplementation reverses hypertrophic car-diomyopathy induced by chronic pressure overload in mice. J Exp Med 204:657–666

33. Nadeem S, Shahzadi I (2015) Inspiration of induced magnetic field on nano hyperbolic tangent fluid in a curved channel. AIP Adv 6:015110

34. Kamel MH, Eldesoky IM, Maher BM, Abumandour RM (2015) Slip effects on peristaltic transport of a particle-fluid suspension in a planar channel. Appl Bion Biomech 2015:14

35. Akram S, Nadeem S (2015) Significance of nanofluid and partial slip on the peristaltic transport of a non-Newtonian fluid with different wave forms. IEEE Trans Nanotechnol 13:375–385

36. Das K (2012) Effects of slip and heat transfer on MHD peristaltic flow in an inclined asymmetric channel. Iran J Math Sci Inform 7:35–52

37. Yildirim Y, Sezer SA (2010) Effects of partial slip on the peristaltic flow of a MHD Newtonian fluid in an asymmetric channel. Math Comput Model 52:618–627